Chapter – III

Growth and Characterization of Lead-Iron Mixed Levo Tartrate Crystals

3.1 Introduction

The growth of several mixed tartrate compounds crystals by the gel technique and their characterization were reported by different workers, for example, mixed iron-manganese levo-tartrate crystals [1], mixed calcium-strontium levo-tartrate crystals [2], mixed iron-manganese-cobalt ternary levo-tartrate crystals [3], mixed iron-manganese-nickel ternary levo-tartrate crystals [4] and mixed calcium-cadmium tartrate single crystals [5]. Apart from these, many other mixed crystals have been grown by different workers using the gel growth; for example, mixed crystals of iron-nickel tartrate as well as iron-cobalt tartrate [6] and mixed crystals of strontium-manganese tartrates [7].

Earlier, iron (II) tartrate crystals [1,8,9] have been successfully grown by the gel growth technique and were characterized using TGA, FTIR and Mössbauer spectroscopy. Similarly, lead tartrate crystals have been successfully grown by gel technique and characterized by FTIR and powder XRD [10,11]. Pure and doped single crystals of lead iodide dihydrate and lead tartrate dihydrate have been successfully grown in silica gel and characterized by Fourier Transform Raman Spectra [12].

This chapter deals with the growth and characterization of pure and mixed lead-iron (Pb-Fe) levo-tartrate crystals. The crystals were characterized by Energy Dispersive Analysis- of X-ray (EDAX), powder X-ray diffraction (XRD), Fourier Transform Infrared (FT-IR) spectroscopy, Thermo Gravimetric Analysis (TGA), impedance spectroscopy, dielectric studies and Vibrating Sample Magnetometer (VSM) study.

3.2 Experimental Techniques

3.2.1 Gel Preparation

In the present case, AR grade sodium meta-silicate powder was used to prepare the gel medium. To prepare the aqueous solution of sodium meta-silicate of 1.05 specific gravity, 100g sodium meta-silicate was dissolved in one litre distilled water in a beaker. This solution was stirred thoroughly and dense milky solution was formed. It was left for a couple of days, so that heavy insoluble impurities could

accumulate at the bottom of the beaker. This was decanted into another beaker and filtered twice with a Whatman (cat No 1001 125) filter paper of 12.5 cm diameter. To get rid off all suspended impurities, the solution was centrifuged on high speed centrifuge unit for about half an hour at 10,000 revolutions per minute, as a result transparent golden colored solution of sodium meta-silicate was obtained for further use to set the gel. The specific gravity of the solution was measured by using standard specific gravity bottles.

3.2.2 Crystal Growth

The single diffusion gel growth technique was used to grow the crystals. Glass test tubes of 25 mm diameter and 140 mm length were used as a crystallization apparatus. The AR grade chemicals were used. To grow mixed Pb-Fe levo tartrate crystals, 1M levo tartaric acid solution was mixed with sodium meta-silicate solution of specific gravity 1.05 in such a manner that 4.5 pH of the mixture could be obtained. The mixture was transferred into different test tubes to set in to the gel form. Within three days the gel was formed. After setting the gel the supernatant solutions consisting of lead nitrate ($Pb(NO_3)_2$) and ferrous nitrate ($Fe(NO_3)_2{\cdot}9H_2O$) solutions having concentrations of 1 molar each were poured gently without disturbing the gel surface.

The compositions of the supernatant solutions were as follows:

(A) 10 ml, 1M, $Pb(NO_3)_2$ …….....sample-1

(B) 2 ml, 1M, $Pb(NO_3)_2$ + 8 ml, 1M, $Fe(NO_3)_2{\cdot}9H_2O$.....sample-2

(C) 4 ml, 1M, $Pb(NO_3)_2$ + 6 ml, 1M, $Fe(NO_3)_2{\cdot}9H_2O$.....sample-3

(D) 6 ml, 1M, $Pb(NO_3)_2$ + 4 ml, 1M, $Fe(NO_3)_2{\cdot}9H_2O$.....sample-4

(E) 8 ml, 1M, $Pb(NO_3)_2$ + 2 ml, 1M, $Fe(NO_3)_2{\cdot}9H_2O$.....sample-5

The following reaction is expected to occur,

$$(1\text{-}X)Pb(NO_3)_{2(aq)} + XFe(NO_3)_2{\cdot}9H_2O_{(aq)} + H_2C_4H_4O_6 + nH_2O$$
$$= Fe_XPb_{(1\text{-}X)}C_4H_4O_6\ nH_2O + 4HNO_3 + 8H_2O + 1/2O_2 \quad (3.1)$$

Where, X = 0.2, 0.4, 0.6 and 0.8.

The supernatant solution (A) is selected for the comparison of mixed crystals with pure lead levo tartrate crystals. The crystal growth was completed within 20 days. The solutions of $Pb(NO_3)_2$ and $Fe(NO_3)_2{\cdot}9H_2O$ were added in such a way that the total volume of the supernatant solution remained constant.

3.3 Crystal growth observation

The following crystal growth observations were made:

(1) Dendrite type, long and dense white crystals were grown at the liquid-gel interface for supernatant solution-A.

(2) No crystal growth is observed for supernatant solution-B. It is because in case of lead nitrate and iron nitrate interacting with tartaric acid, reaction of lead prominent giving major lead tartrate products with very less iron content. It can be concluded from this result that iron nitrate having oxidizing characteristics resists itself to form composition with tartaric acid in presence of lead. It is shown in figure (3.1b).

(3) Figure (3.1c) shows the crystal growth for supernatant solution-C. Dendrite type, short and very less dense reddish crystals were grown at the liquid-gel interface.

(4) Figure (3.1d) shows the crystal growth in the test tube for the supernatant solution-D. At the liquid-gel interface, dendrite types, short, dense and reddish in color crystals were grown.

(5) Compared to supernatant solutions C and D, the longer, dendrite type, very dense and less reddish color crystals were grown at the gel-liquid interface for supernatant solution-E.

(3.1a) **(3.1b)** **(3.1c)** **(3.1d)** **(3.1e)**

Figure (3.1): Growth of crystals in test tubes

Almost in all cases a clear gel was found bellow the liquid-gel interface, which may be due to having not enough number of cations and anions to form the product. As amount of $Pb(NO_3)_2$ in the supernatant solutions was increased, the coloration of the crystals changed from dark reddish to light reddish, density of the number of

grown crystals as well as length of the crystals was increased. This might be due to high reactivity of Pb than Fe.

The mechanism of dendrite formation is already discussed in section 1.8 of chapter-I.

3.4 Characterization of Crystals

3.4.1 EDAX study

In order to find out the elemental composition of the grown crystals, the EDAX study was carried out on grown crystals.

As the sample-1 is pure lead levo tartrate sample, the EDAX spectra were not recorded. The EDAX spectra are shown in figures (3.2) (a) to (c) for different mixed Pb-Fe levo tartrate samples, i.e., from sample-3 to sample-5, respectively. Expected and observed atomic % values are tabulated in table (3.1).

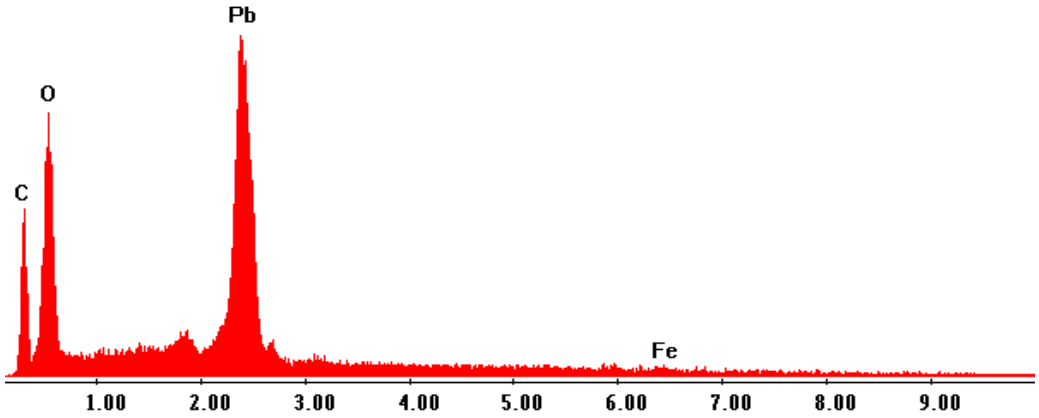

Figure (3.2a): The EDAX spectrum for sample-3

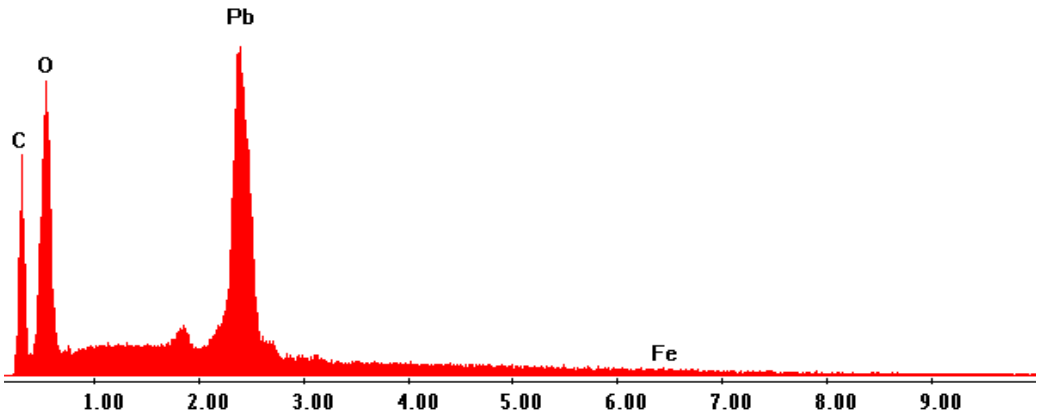

Figure (3.2b): The EDAX spectrum for sample-4

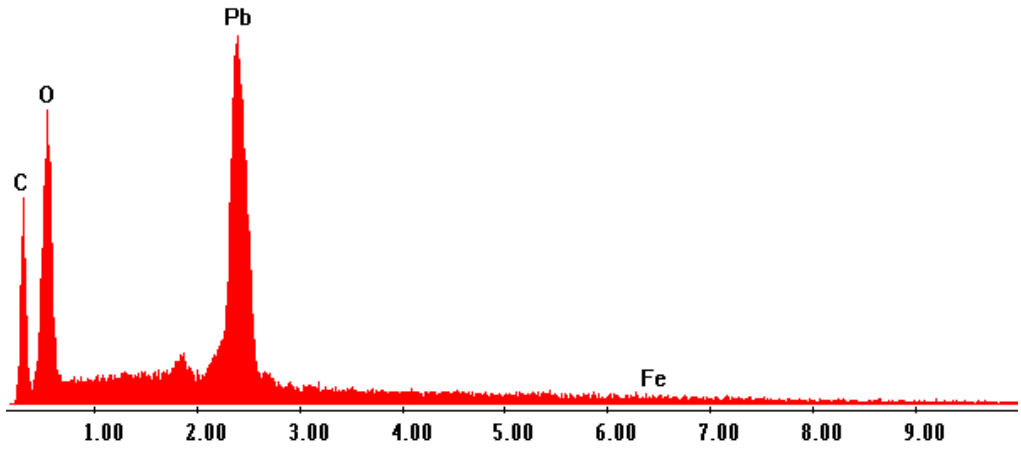

Figure (3.2c): The EDAX spectrum for sample-5

One can find from figures (3.2) (a) to (c) that the elemental contribution of O and C is due to the presence of tartrate ions and water of hydration.

From table (3.1) one can notice that the expected and observed values of the atomic weight percentages of lead and iron in the grown crystals do not match exactly. In the crystalline lattice, due to difference in hydrated and non-hydrated radii of lead and iron, they do not take positions exactly as it has been estimated. It can also be noticed that lead enters the crystalline lattice readily than iron. The reason can be explained on the basis of hydrated radii. In the solution, Pb^{+2} and Fe^{+2} ions possess a primary hydration shell, which is the number of water molecules directly coordinated to both the metal ions. There is also overall solvation number, which is defined as the total number of water molecules associated when the solvent is water, on which both the ions exercise a substantial restraining influence. Then the successive layers of water molecules are termed as the secondary hydration layers. Hydration of an ion depends on the electrostatic attraction of water molecules to that ion. Attraction of water molecules around an ion depends on the density of charge of ion. The smaller ions having greater ionic potential attract more water molecules. The result is the inverse relationship between non-hydrated radius and hydrated radius. In this study, the non-hydrated radius of Pb^{+2} is 1.19 Å and second ionization potential is 15.028 eV, while the same quantities for Fe^{+2} are 0.55 Å and 16.18 eV, respectively. Therefore, the reverse nature is observed for hydrated radii of Pb^{+2} and Fe^{+2} than that for the non-hydrated ones [13,14]. As the hydrated radii of Pb^{+2} being smaller than the hydrated radii of Fe^{+2}, the Pb^{+2} ions enter into the reaction in higher concentration

than Fe^{+2} ions, which is resulting higher concentration of Pb in grown crystals than Fe.

The proposed formula and the estimated formula for the relevant crystals are given in the following table (3.2).

Table (3.1): EDAX result for Pb-Fe mixed levo tartrate crystals

Sample No.	Sample	Expected Atomic Weight (%)		Observed Atomic Weight (%) (From EDAX)	
		Element		Element	
		Pb	Fe	Pb	Fe
1.	$PbC_4H_4O_6 \cdot nH_2O$	100	0	-	-
2.	$Pb_{0.2}Fe_{0.8}C_4H_4O_6 \cdot nH_2O$	20	80	-	-
3.	$Pb_{0.4}Fe_{0.6}C_4H_4O_6 \cdot nH_2O$	40	60	98.93	1.07
4.	$Pb_{0.6}Fe_{0.4}C_4H_4O_6 \cdot nH_2O$	60	40	99.36	0.64
5.	$Pb_{0.8}Fe_{0.2}C_4H_4O_6 \cdot nH_2O$	80	20	99.38	0.62

Table (3.2): Proposed and estimated formula for Pb-Fe mixed levo tartrate crystals

Sample No.	Proposed formula for the Sample	Estimated formula from the EDAX
1	$PbC_4H_4O_6 \cdot nH_2O$	$PbC_4H_4O_6 \cdot nH_2O$
2	$Pb_{0.2}Fe_{0.8}C_4H_4O_6 \cdot nH_2O$	-
3	$Pb_{0.4}Fe_{0.6}C_4H_4O_6 \cdot nH_2O$	$Pb_{0.989}Fe_{0.011}C_4H_4O_6 \cdot nH_2O$
4	$Pb_{0.6}Fe_{0.4}C_4H_4O_6 \cdot nH_2O$	$Pb_{0.993}Fe_{0.007}C_4H_4O_6 \cdot nH_2O$
5	$Pb_{0.8}Fe_{0.2}C_4H_4O_6 \cdot nH_2O$	$Pb_{0.994}Fe_{0.006}C_4H_4O_6 \cdot nH_2O$

In the present chapter the formulae for mixed Pb-Fe levo tartrate compounds are used as per given in table (3.2).

3.4.2 Powder XRD study

The mixed crystals of metal tartrate compounds have been studied by using powder XRD by several authors, for example, mixed iron-manganese-cobalt ternary levo tartrate crystals [3] and mixed iron-nickel-manganese ternary levo tartrate crystals [4]. Kansara [7] has studied the pure and mixed tartrate crystals of manganese and strontium and found that the unit cell parameters prefer the values according to

the content involved in the sample. It has been observed by Kansara [7] that in case of higher strontium content the mixed crystals attain almost the crystal structure as well as the unit cell parameters of strontium tartrate and the sudden flip is observed as the content of manganese increases in the mixed crystals and opt for crystal structure of manganese tartrate. Whereas, Joseph [6] has studied the mixed crystals of iron-nickel and iron-cobalt tartrate and found no systematic variation in the unit cell parameters values of the crystals and they almost retain the structure of iron tartrate crystals. Recently, Joshi et al [15] have reported that in mixed Mn-Cu levo-tartrate crystals as the amount of Cu increases the value of parameter-c of the unit cell tries to adopt the value that of the pure copper levo-tartrate crystal.

In the present study, an attempt is made to find out the effect of proportion of lead and iron in the mixed Pb-Fe levo tartrate crystals in the perspective of structural changes.

Figures (3.3) (a) to (d) indicate powder X-ray diffraction patterns of pure and mixed lead-iron levo tartrate crystals. The cell parameters were obtained by computer software Powder-X, which are tabulated in table (3.3).

The orthorhombic unit cell parameters of lead tartrate crystals are: a = 7.99482 Å, b = 8.84525 Å, c = 8.35318 Å with space group $P2_12_12_1$ [16], while the orthorhombic unit cell parameters of iron tartrate crystals are a = 8.7588 Å, b = 10.9889 Å, c = 8.1900 Å [1]. Comparing with the pattern of pure lead tartrate, it is observed that the intensity of all the peaks of mixed crystals of Pb and Fe is reduced without significant change in the peak position of the pattern of pure lead levo tartrate. The scattering intensities for X-rays are directly related to the number of electrons in the atom. Hence, light atoms scatter X-rays weakly, while heavy atoms scatter X-rays more effectively. Therefore, doping of light element, i.e., Fe, reduces the intensity of peaks. The percentage weight of iron in the structure of mixed crystals of lead and iron levo-tartrate is very less and, therefore, the unit cell parameters of mixed crystals are close to the unit cell parameters of pure lead levo-tartrate. It is also observed that the most intense peaks of pure lead levo tartrate (020) at 21.12°, (022) at 29.44°, (031) at 32.25°, (131) at 34.17°, (311) at 36.25°, (040) at 40.88°, (033) at 44.71°, and (261) at 68.79° are shifted very little from their positions. This indicates that there is no strain produced in the structure of pure lead tartrate due to doping of iron because of low ionic radius of iron (0.55 Å) compared to lead (1.19 Å) [17].

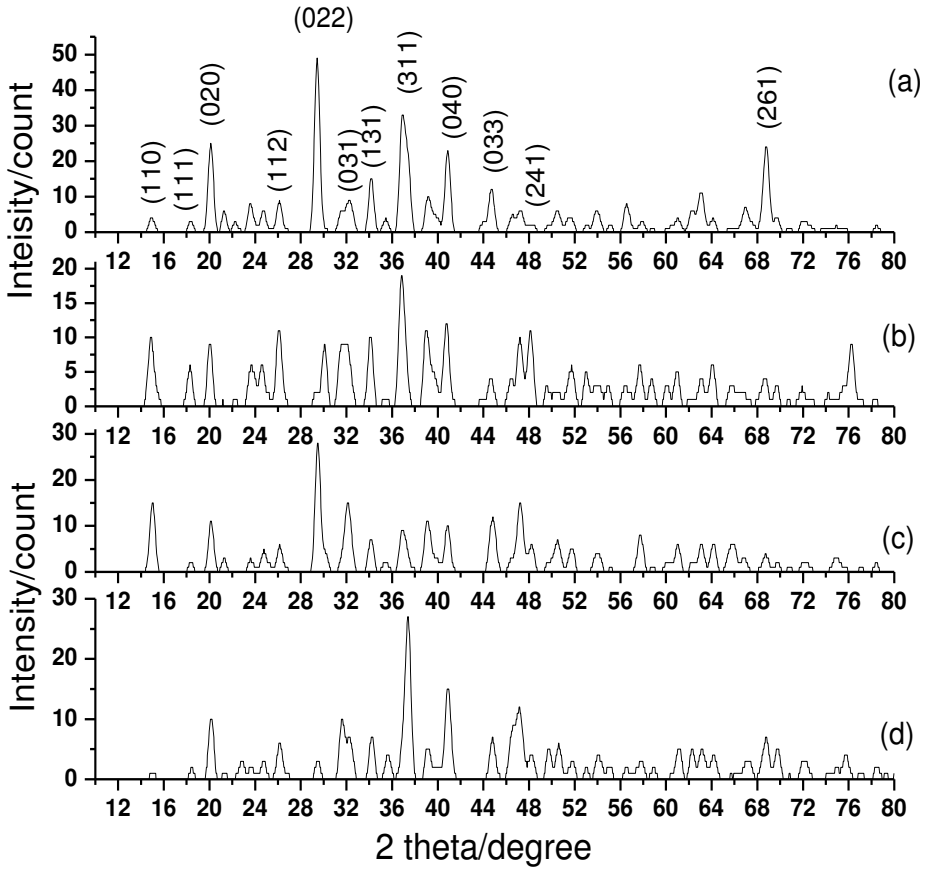

Figure (3.3): The powder XRD patterns for (a) $PbC_4H_4O_6 \cdot nH_2O$ (b) $Pb_{0.989}Fe_{0.011}C_4H_4O_6 \cdot nH_2O$ (c) $Pb_{0.993}Fe_{0.007}C_4H_4O_6 \cdot nH_2O$ (d) $Pb_{0.994}Fe_{0.006}C_4H_4O_6 \cdot nH_2O$

Table (3.3): The cell parameters for Pb-Fe levo tartrate crystals with α=β=γ=90°

Sample No.	Sample	Unit cell parameters		
		a (Å)	b (Å)	c (Å)
1	$PbC_4H_4O_6 \cdot nH_2O$	7.99	8.84	8.35
2	Not formed	-	-	-
3	$Pb_{0.989}Fe_{0.011}C_4H_4O_6 \cdot nH_2O$	8.0048	8.8452	8.3532
4	$Pb_{0.993}Fe_{0.007}C_4H_4O_6 \cdot nH_2O$	7.9820	8.8400	8.3550
5	$Pb_{0.994}Fe_{0.006}C_4H_4O_6 \cdot nH_2O$	7.9920	8.8500	8.3540

The peaks of Fe are not separately identified in the mixed crystals of Pb and Fe, which may be due to very less percentage of iron in the mixed crystals. From table (3.3), one can find that the pure lead levo-tartrate crystals of sample (1), as well as mixed Pb-Fe levo tartrate crystals of sample (3-5) exhibit orthorhombic structure. The unit cell parameter values of lead and iron mixed tartrate crystals is closer to the unit cell parameters values of pure lead tartrate, which indicates that the less amount of iron in the mixed crystals has no significant influence on the unit cell dimensions.

3.4.3 FTIR Spectroscopy study

From the earliest days of infrared spectroscopy it was observed that functional groups of atoms could be associated with definite characteristic absorption bands, i.e., the absorption of infrared radiation over certain frequency intervals. The infrared spectrum of any given substance is interpreted by the use of the known group frequencies and thus it will be easy to characterize the substance as one containing a given type of group or groups. Although group frequencies occur within narrow limits, interference or perturbation may cause a shift of the characteristic bands due to (a) the electro negativity of neighboring groups or atoms, (b) the spatial geometry of the molecule, or (c) the mechanical mixing of vibrational modes.

Functional groups sometimes have more than one characteristic absorption band associated with them. On the other hand, two or more functional groups may absorb in the same region and hence, in general, can only be distinguished from each other by means of other characteristic infrared bands, which occur in non-over lapping regions.

Absorption bands may be considered as having two origins, these being the fundamental vibrations of (a) functional groups, e.g. C=O, C=C, C≡N, -CH2-, -CH3-, and (b) skeletal groups, i.e. the molecular backbone or skeleton of the molecule e.g., C-C-C-C. Absorption bands may also arise from stretching vibrations, i.e., vibrations involving bond-length changes, or deformation vibration, i.e., vibrations involving bond-angle changes, of the group. Each of these, in some cases, may be considered as arising from symmetric or asymmetric vibrations.

For a given functional group, the vibration bands due to stretching occur at higher frequencies than those due to deformation. This is because more energy is required to stretch the group than to deform it due to the bonding force directly opposing the change.

Earlier, Bolard [18] obtained the infrared spectra of tartaric acid and some simple tartrates. Sheveheko [19] studied the IR spectra of both normal and partially deuterated compounds of some tartrates and found absorptions at 600 cm^{-1} and 400 cm^{-1} due to COO^- group in metal tartrates. The formula of metal tartrate was suggested as follows.

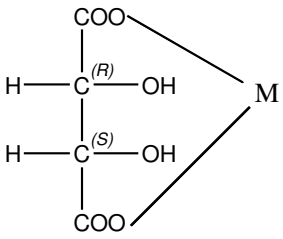

Figure (3.5): structural diagram

Patel et al [20] considered the magnetic susceptibility data and FTIR spectrum for ferrous tartrate and suggested an octahedral environment around Fe-atom. They propose the empirical formula $FeC_4H_4O_6 \cdot 2.5\ H_2O$. The magnetic susceptibility value of 5.4 BM indicated an octahedral environment around Fe(II) [21] and hence they suggested a molecular formula $FeC_4H_4O_6 \cdot 5\ H_2O$ so that six coordination of Fe(II) is satisfied. By considering the infra-red data, they proposed the structure as shown in figure (3.6).

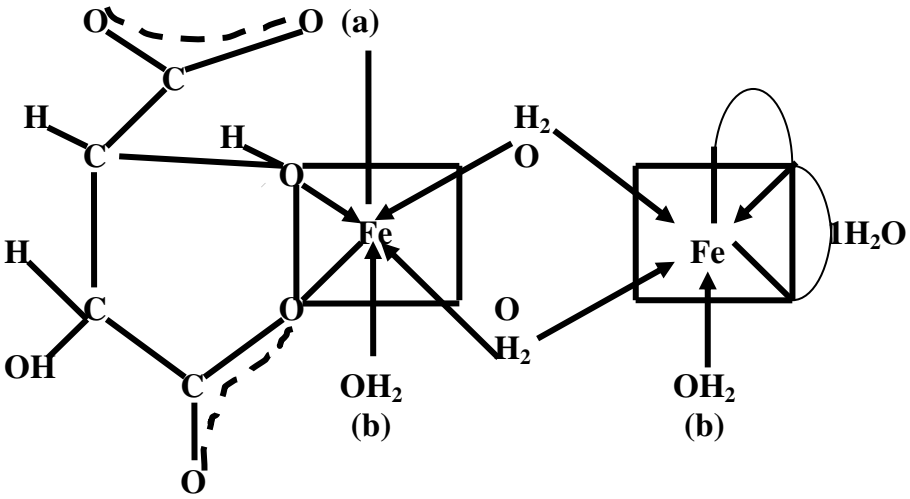

Figure (3.6): The proposed structure

The two bridged water molecules and the two Fe (II) ions are proposed to be in the same plane. The oxygen atoms, designated as (a), are lying the plane while the molecules designated as (b) below the plane, thus satisfying the six coordination of

each Fe(II). For each Fe($C_4H_4O_6$) unit 2.0m are the water of coordination and 0.5m is the water of crystallization.

Many workers have studied and reported the FT-IR spectra of different tartrate compounds, for example, mixed iron-manganese-cobalt ternary levo tartrate crystals [3], mixed iron-nickel-manganese ternary levo tartrate crystals [4], mixed Ca-Sr levo-tartrate crystals [2], Fe-Ni and Fe-Co mixed levo-tartrates [6], Mn-Fe levo-tartrate crystals [22] and recently on Mn-Cu levo-tartrate [15]. Here, the present author reports the FTIR spectroscopy study of pure and mixed Pb-Fe levo-tartrate crystals. The spectra were recorded within 400-4000 cm^{-1} range.

Figure (3.7) shows FTIR spectra of pure and mixed Pb-Fe levo-tartrate and the table (3.4) gives the assignments of various absorptions.

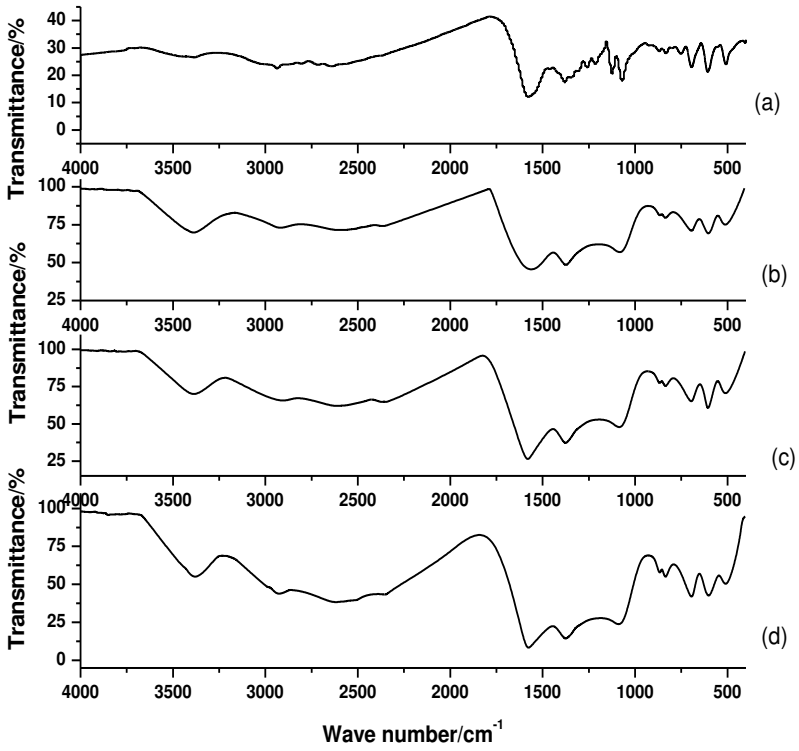

Figure (3.7): FTIR spectra (a) Sample 1. Pure Pb levo-tartrate (b) Sample 3. $Pb_{0.989}Fe_{0.011}C_4H_4O_6{\cdot}nH_2O$ (c) Sample 4. $Pb_{0.993}Fe_{0.007}C_4H_4O_6{\cdot}nH_2O$ and (d) Sample 5. $Pb_{0.994}Fe_{0.006}C_4H_4O_6{\cdot}nH_2O$

One can find from the spectra that the absorptions taking place around 3380 cm^{-1} is due to water of crystallization associated with the crystals. The C=O group stretching vibrations are observed around 1590 cm^{-1}. The bonded O-H stretching

vibrations occur from 2630 cm^{-1} to 2936 cm^{-1}. The C-H stretching asymmetrical vibrations and C-H banding vibrations occur around 2930 cm^{-1} and 1380 cm^{-1}, respectively. The C-O stretching vibrations and C-C bending vibrations are observed around 1125 cm^{-1} and 835 cm^{-1}, respectively. The metal oxygen vibrations occur below 700 cm^{-1}. This proves the presence of O-H, C=O, C-H, C-O functional groups and metal-oxygen bonding.

Comparing the different absorptions of mixed Pb-Fe levo-tartrate crystals in FTIR spectra with the pure lead tartrate crystals, one can conclude that there is no major effect of iron on the different absorptions in FTIR spectra. This may be due to very less amount of iron present in the mixed crystals of Pb-Fe levo-tartrate.

Table (3.4): FTIR spectral data

Assignments	Wave number (cm^{-1})			
	Sample (1)	Sample (3)	Sample (4)	Sample (5)
Free O-H Stretching	3384.9	3380.04	3380.60	3380.31
C-H Stretching (asymmetrical)	2936.40	2930.86	2932.42	2933.93
Bonded O-H Stretching	2637.00	2632.15	2632.84	2936.60
C=O Stretching	1571.20	1594.15	1593.88	1592.91
C-H Banding (Alkane)	1382.30	1383.06	1383.04	1383.01
C-O Stretching	1128.00	1127.77	1128.00	1128.14
C-C Bending	836.90	835.66	835.87	835.74
Pb-O and Fe-O Stretching	696.50, 605.40, 513.80	680.06, 604.03, 513.08	695.59, 604.40, 513.48	695.34, 604.08, 512.80

Atomic mass number of lead and iron is 207 and 56, respectively. From table (3.4), it is observed that as the iron is doped into the lead, the shift is found towards lower frequency that indicates low energy is required for vibrations. This indicates clearly the mixed nature of the lead-iron levo-tartrate. For example, the metal-oxygen vibration as well as O-H stretching vibration in pure lead tartrate shifts towards slightly lowers frequency side in the mixed Pb-Fe levo-tartrate crystals. The presence of the less massive Fe is expected to cause alternations in the molecular geometry, bond length and mechanical vibrations and as a result the absorption spectra are slightly altered. This also indicates that the metal ion is coordinated with water molecule through O-H bonding and having metal-oxygen bonding.

3.4.4 Thermal Study

In TGA, the weight of a sample in a controlled atmosphere is recorded continuously as a function of temperature or time, as the temperature of the sample is increased (usually linearly with time). A plot of mass or mass percent as a function of temperature is called a thermogram, or a thermal decomposition curve, or a pyrolysis curve. Often a pyrolysis occurs through many-stepped mechanisms, where the temperature ranges for each step overlap, resulting in irregular weight-temperature curve that may be difficult to analyze. Also, in many cases the trace follows a characteristics path common to a wide range of decomposition processes, which includes many polymer pyrolysis. The sample weight drops slowly as pyrolysis begins, then drops precipitously over a narrow range of temperature and finally turn back to zero slope as the reactants are used up.

Many researchers have reported the thermal study of various tartrate compounds, e.g., iron (II) tartrate [6], iron-nickel mixed tartrate [6], ytterbium tartrate trihydrate [23] mixed iron-manganese levo-tartrate [1], pure and mixed levo-tartrates of calcium and strontium [2], mixed iron-manganese-cobalt ternary levo-tartrate [3], mixed iron-nickel-manganese ternary levo-tartrate [4]. A mixed calcium-cadmium tartrate [5] and Mn-Fe mixed levo-tartrate [22] have been reported. Rodrigues et al [24] studied some bivalent tartrate compounds and on the basis of DTA, TGA and DSC concluded that the thermal stability of compounds depends on the nature of metal ions and it follows the order as: Zn>Cu>Mn = Co>Ni>Fe.

In the present study, Pb-Fe mixed levo-tartrate crystals have been grown and characterized for the thermal stability by thermo-gravimetry analysis.

Figure (3.8) shows the thermo-gram of $PbC_4H_4O_6{\cdot}nH_2O$, $Pb_{0.989}Fe_{0.011}C_4H_4O_6{\cdot}nH_2O$, $Pb_{0.993}Fe_{0.007}C_4H_4O_6{\cdot}nH_2O$ and $Pb_{0.994}Fe_{0.006}C_4H_4O_6{\cdot}nH_2O$ crystals, respectively. Table (3.5) shows the theoretical and experimental mass loss values with the reactions involved at each stage of decomposition of the samples.

Figure (3.8 a) shows the thermo-gram of the $PbC_4H_4O_6.nH_2O$ crystal, which indicates that the compound is stable up to 200°C and then starts losing crystalline water and becomes anhydrous at 240°C after losing approximately 10 % weight of its original weight. During the second stage of decomposition between 240°C to 300°C, the sample is converted into carbonate form with the loss of nearly further 33 % of its original weight. During the third and final stage of decomposition between 300°C to

600°C, the sample is converted into oxide form with the loss of nearly 43 % of its original weight. From the analysis it is found that 2.4 water molecules are associated with the crystal.

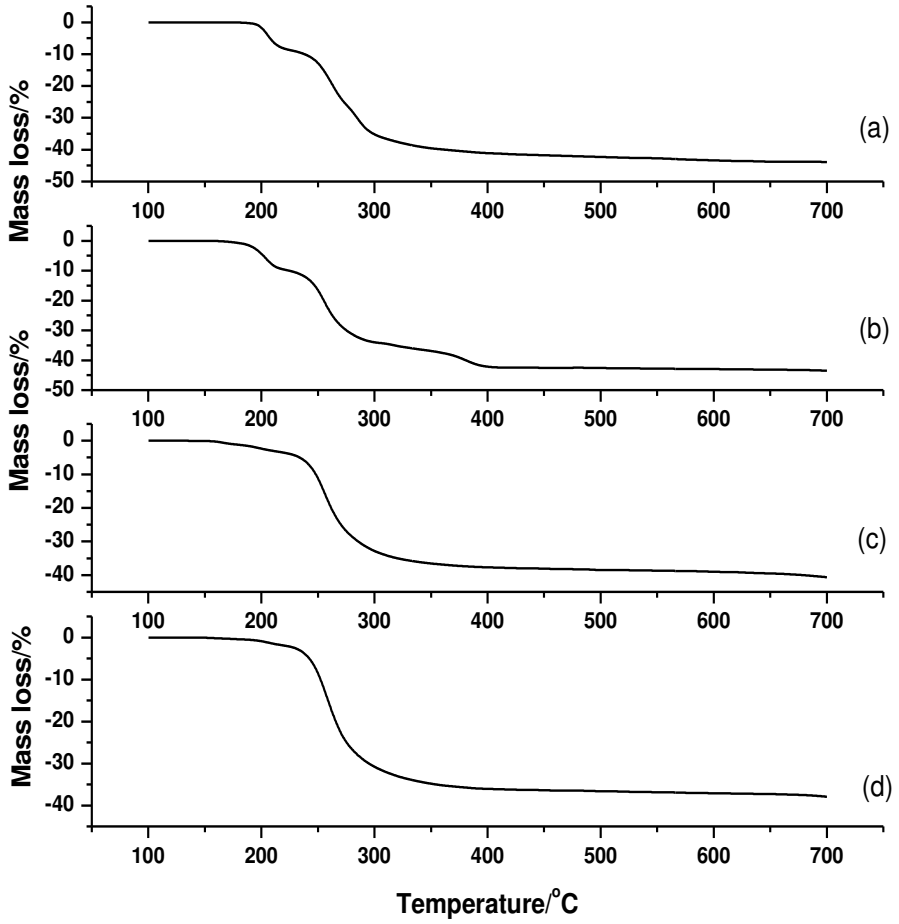

Figure (3.8): Thermo-grams of (a) Sample 1. $PbC_4H_4O_6 \cdot nH_2O$ (b) Sample 3. $Pb_{0.989}Fe_{0.011}C_4H_4O_6 \cdot nH_2O$ (c) Sample 4. $Pb_{0.993}Fe_{0.007}C_4H_4O_6 \cdot nH_2O$ and (d) Sample 5. $Pb_{0.994}Fe_{0.006}C_4H_4O_6 \cdot nH_2O$

Figures (3.8 b-d) show the thermo-grams of the samples (3-5), respectively. The first stage of dehydration occurs between 170°C and 210°C for sample (2) and between 160°C and 200°C for the samples (4-5), which results into formation of anhydrous lead-iron mixed tartrate. During the second stage between 210°C and 280°C for sample (2), 200°C and 270°C for sample (3) and 200°C and 280°C for sample (5), the anhydrous sample is converted into carbonate form. During the third and final stage of decomposition between 280°C and 400°C for sample (3 and 5) and between 270°C and 400°C for sample (4), the sample is converted into oxide form. The amount of

water molecules attached with samples (1, 3, 4 and 5) have been calculated and found to be 2.4, 1.9, 0.5 and 0.17, respectively. The correct stoichiometric formula for the pure Pb tartrate crystals as well as for the Pb-Fe mixed levo-tartrate crystals are listed in the table 3.6 after the EDAX and TGA study.

Table (3.5): Theoretical and experimental mass loss values with reactions involved

Sample	Temperature (^oC)	Reactions involved	Theoretical mass loss (%)	Experimental mass loss (%)
Sample (1)	50 – 200	No decomposition	100	100
	200 – 240	$PbC_4H_4O_6\ 2.4H_2O \rightarrow PbC_4H_4O_6 + 2.4H_2O$	10.85	9.07
	240 – 300	$PbC_4H_4O_6 \rightarrow PbCO_3 + CH_4 + 2CO + ½\ O_2$	32.95	35.41
	300 – 600	$PbCO_3 \rightarrow PbO + CO_2$	44.00	43.25
Sample (3)	50 – 170	No decomposition	100	100
	170 – 210	$Pb_{0.989}Fe_{0.011}C_4H_4O_6\ 1.9H_2O \rightarrow Pb_{0.989}Fe_{0.011}C_4H_4O_6 + 1.9H_2O$	8.83	8.77
	210 – 280	$Pb_{0.989}Fe_{0.011}C_4H_4O_6 \rightarrow Pb_{0.989}Fe_{0.011}\ CO_3 + CH_4 + 2CO + 1/2\ O_2$	31.53	31.32
	280 – 400	$Pb_{0.989}Fe_{0.011}CO_3 \rightarrow Pb_{0.989}Fe_{0.011}O + CO_2$	42.89	42.27
Sample (4)	50 – 160	No decomposition	100	100
	160 – 200	$Pb_{0.993}Fe_{0.007}C_4H_4O_6\ 0.5H_2O \rightarrow Pb_{0.993}Fe_{0.007}C_4H_4O_6 + 0.5H_2O$	2.48	2.40
	200 – 270	$Pb_{0.993}Fe_{0.007}C_4H_4O_6 \rightarrow Pb_{0.993}Fe_{0.007}\ CO_3 + CH_4 + 2CO + 1/2O_2$	26.72	25.40
	270 – 400	$Pb_{0.993}Fe_{0.007}CO_3 \rightarrow Pb_{0.993}Fe_{0.007}O + CO_2$	38.84	37.66
Sample (5)	50 – 160	No decomposition	100	100
	160 – 200	$Pb_{0.994}Fe_{0.006}C_4H_4O_6\ 0.17H_2O \rightarrow Pb_{0.994}Fe_{0.006}C_4H_4O_6 + 0.17H_2O$	0.86	0.89
	200 – 280	$Pb_{0.994}Fe_{0.006}C_4H_4O_6 \rightarrow Pb_{0.994}Fe_{0.006}CO_3 + CH_4 + 2CO + 1/2O_2$	25.50	26.77
	280 – 400	$Pb_{0.994}Fe_{0.006}CO_3 \rightarrow Pb_{0.994}Fe_{0.006}O + CO_2$	37.83	36.07

Table (3.6): The correct stiochiometric formula

Sample	The correct stiochiometric formula from TGA
Sample (1)	$PbC_4H_4O_6\ 2.4H_2O$
Sample (3)	$Pb_{0.989}Fe_{0.011}C_4H_4O_6\ 1.9H_2O$
Sample (4)	$Pb_{0.993}Fe_{0.007}C_4H_4O_6\ 0.5H_2O$
Sample (5)	$Pb_{0.994}Fe_{0.006}C_4H_4O_6\ 0.17H_2O$

Vohra [22] as well as Joshi et al [1] have studied thermo-gravimetry analysis of pure and mixed Mn-Fe levo tartrate crystals of $MnC_4H_4O_6{\cdot}1.5H_2O$, $Mn_{0.68}Fe_{0.32}C_4H_4O_6{\cdot}2H_2O$, $Mn_{0.22}Fe_{0.78}C_4H_4O_6{\cdot}2H_2O$, $Mn_{0.15}Fe_{0.85}C_4H_4O_6{\cdot}2.5H_2O$ and $FeC_4H_4O_6{\cdot}2.5H_2O$ compositions. It was found that in these samples the occurrence of dehydration is from 125°C to 135°C and final oxide state beyond 435 °C. Altogether, Parikh et al [2] observed the clear effect of increase in calcium content on the thermo-grams of mixed calcium-strontium levo-tartrate crystals. In the present case, the occurrence of dehydration is from 200 ^oC to 240 ^oC and final oxide state is from 300 ^oC to 600 ^oC for pure lead tartrate crystals. In the present study, on moving from pure Pb levo tartrate crystal to mixed Pb-Fe levo-tartrate crystals, the stage of dehydration as well as the stage of oxide was achieved with decreasing order of temperature with minor change in the respective temperature values. This is due to very low percentage values of iron in the mixed crystals.

In the remaining discussion, the estimated formulae for the pure and mixed Pb-Fe levo-tartrate crystals are used as mentioned in the table (3.6).

3.4.5 Differential Thermal Analysis and Differential Scanning Calorimetry

Differential Thermal Analysis (DTA) is the analytical technique in which the temperature differential between the sample and a nonreactive reference material is monitored while the two substances are subjected to the identical heating program. Unlike TG, DTA does not require a change in mass of the sample in order to obtain meaningful information. DTA can be used to study any process in which heat is absorbed or evolved. Among the endothermic processes that can be studied using DTA are melting, boiling and sublimation. Absorptive processes are often exothermic and can be studied by using DTA. Thermal curves obtained with DTA show peaks corresponding to processes in which the temperature of the sample is increased or decreased relative to the temperature of the reference substance. Upward deflection usually corresponds to exothermic reactions and downward deflection to endothermic

reaction. The temperatures at which the peaks are observed in thermal curve can be used for qualitative analysis.

Differential Scanning Calorimetry (DSC) is the technique in which the temperatures of a sample and reference substance are controlled at identical values while the amount of heat that is added to the other substance is monitored. DSC can be used to measure enthalpimetric changes associated with physical and chemical transitions.

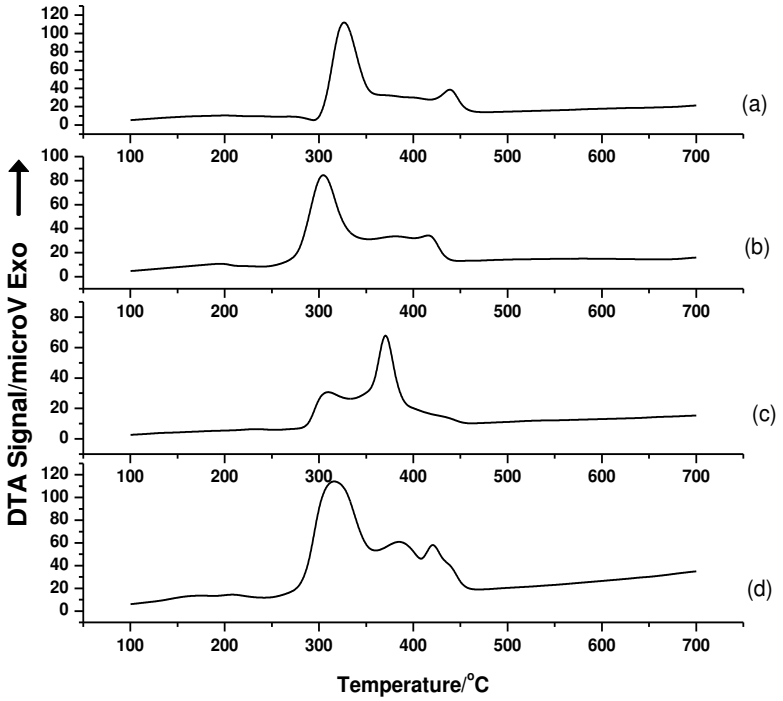

Figure (3.9): DTA curves of (a) Sample 1. $PbC_4H_4O_6{\cdot}2.4H_2O$ (b) Sample 3. $Pb_{0.989}Fe_{0.11}C_4H_4O_6{\cdot}1.9H_2O$ (c) Sample 4. $Pb_{0.993}Fe_{0.007}C_4H_4O_6{\cdot}0.5H_2O$ and (d) Sample 5. $Pb_{0.994}Fe_{0.006}C_4H_4O_6{\cdot}0.17H_2O$

Figure (3.9) shows the DTA curves of $PbC_4H_4O_6{\cdot}nH_2O$, $Pb_{0.989}Fe_{0.011}C_4H_4O_6{\cdot}1.9H_2O$, $Pb_{0.993}Fe_{0.007}C_4H_4O_6{\cdot}0.5H_2O$ and $Pb_{0.994}Fe_{0.006}C_4H_4O_6{\cdot}0.17H_2O$ crystals, respectively.

The DTA plot of figure (3.9 a) indicates that the decomposition process of pure Pb levo-tartrate occurs through two exothermic reactions at 326.4^oC and 440.1^oC, respectively. From the DSC plot several thermodynamic parameters were calculated by using the software TA evaluation available with the set up. For the first exothermic reaction at 326.4^oC, the enthalpy, the change in heat capacity and the heat change are calculated and found to be 1134.49 J/g, 8.75 J/gK and 498.21 μVs/mg,

respectively. This may be due to decomposition of sample into carbonate form. For the second exothermic reaction at 440.1°C, the values of enthalpy, change in heat capacity and heat change are found to be 155.58 J/g, 2.17 J/gK and 53.54 μVs/mg, respectively. This may be due to decomposition of the sample into oxide form.

The DTA plot of figure (3.9 b) indicates the decomposition process of sample $Pb_{0.989}Fe_{0.011}C_4H_4O_6 \cdot 1.9H_2O$. It can be noticed from the plot that there are two exothermic peaks associated with the decomposition of a sample. The first sharp exothermic peak is observed at temperature 304.9°C with the change in enthalpy, change in heat capacity and heat change are 777.92 J/g, 3.75 J/gK and 353.83 μVs/mg, respectively. The occurrence of this exothermic reaction may be due to decomposition of sample into carbonate form. The second exothermic peak is observed at temperature 414.0°C. The values of enthalpy, change in heat capacity and heat change are found to be 93.84 J/g, 4.26 J/gk and 26.55 μVs/mg, respectively. This exothermic reaction may be associated with the decomposition of sample into oxide form.

The DTA plot of figure (3.9) shows the two exothermic reactions for $Pb_{0.993}Fe_{0.007}C_4H_4O_6 \cdot 0.5H_2O$ sample. The first exothermic reaction occurs at 301.4°C due to the conversion of anhydrous sample into carbonate form. The second exothermic reaction occurring at 429.6°C is due to conversion into oxide form. The values of different thermodynamic and heat parameters are given in the table (3.7) for the two exothermic reactions.

The DTA curve of the sample $Pb_{0.994}Fe_{0.006}C_4H_4O_6 \cdot 0.17H_2O$ is shown in figure (3.9 d) exhibiting two exothermic reactions at temperature 315.9°C and 421.5°C, respectively. The first exothermic reaction at 315.9°C may be due to conversion of anhydrous sample into carbonate form. The second exothermic reaction at temperature 421.5°C may be due to conversion of sample into oxide form. The values of enthalpy and change in heat capacity are given in table (3.7) for both reactions.

It can be noticed from the table (3.7) that the lowest value of enthalpy for the carbonate stage is obtained for the sample $Pb_{0.993}Fe_{0.007}C_4H_4O_6 \cdot 0.5H_2O$, which indicates meta-stable or briefly stable carbonate stage in this sample. While the higher value of enthalpy for the carbonate stage is obtained for the sample $PbC_4H_4O_6 \cdot 2.4H_2O$ and $Pb_{0.994}Fe_{0.006}C_4H_4O_6 \cdot 0.17H_2O$, which indicates highly energetic carbonate stage in these samples.

Table (3.7): Thermodynamic parameters values for pure and mixed Pb-Fe levo tartrate crystals

Sample name	Related stage of decomposition	Temperature (°C)	Enthalpy (J/g)	Change in heat capacity (J/g/K)
$PbC_4H_4O_6 \cdot 2.4H_2O$	carbonate	326.4	1134.48	8.75
	oxide	440.1	155.58	2.17
$Pb_{0.989}Fe_{0.011}C_4H_4O_6 \cdot 1.9H_2O$	carbonate	304.9	777.92	3.75
	oxide	414.0	93.84	4.26
$Pb_{0.993}Fe_{0.007}C_4H_4O_6 \cdot 0.5H_2O$	carbonate	301.4	726.05	1.76
	oxide	429.6	86.75	3.39
$Pb_{0.994}Fe_{0.006}C_4H_4O_6 \cdot 0.17H_2O$	carbonate	315.9	1361.33	10.32
	oxide	421.5	101.08	2.39

3.4.6 Impedance Spectroscopy

Electrical applications of solid state materials covers the complete spectrum from electrical insulators to superconductors. The properties are subdivided into four main categories by Sinclair [25] as follows:

(i) Intra-granular or 'bulk' properties

(ii) Inter-granular or 'grain boundaries' properties

(iii) A combination of both inter and intra granular properties

(iv) Surface properties

In an ac electrical properties of materials the four basic properties are defined as:

(i) Impedance Z^*

$Z^* = Z'(\text{resistive}) - jZ''(\text{reactive})$

(ii) Complex admittance Y^*

$Y^* = (Z^*)^{-1} = Y' + Y''$

Y' = conductivity = σ

(iii) Complex electrical modulus M^*

$M^* = j\omega C_o Z^* = M' + M''$

C_o = vacuum capacitor = $\varepsilon_o A/l$, A = Area, l = separation length, ε_o = permittivity of free space = 8.854×10^{-14} F cm^{-1}

(iv) Complex permittivity ε^*

$\varepsilon^* = (M^*)^{-1} = Y^*(j\omega C_o)^{-1} = \varepsilon' + \varepsilon''$

These four basic formulations are interrelated and they can be subdivided into two sets: (Z^*, M^*) and (Y^*, ε^*). The main advantage of the transformation within each set is to exchange the real and imaginary components simply on multiplication by ω. This makes all four formulations valuable as they have different dependence on ω. Various polarization and charge transfer processes occurring in a test system within the measured frequency range are highlighted by these different formulations, which is very important in the studies of electrical properties of matter.

Sinclair [25] has summarized various forms in which the data are plotted:

(i) A locus of points in the complex plane, i.e., imaginary component against the real component.

(ii) A spectroscopic plot, i.e., the real as well as the imaginary components as a function of *log(f)*.

(iii) A combined spectroscopic plot, i.e., the real or imaginary components of the different formulations as a function of *log(f)*.

(iv) A three dimensional plot with *log(f)* perpendicular to the complex plane.

The majority of the workers present the ac response only in the ε^* and Z^* planes, respectively.

The different regions of test samples are generally characterized by resistance and capacitance connected in parallel. The characteristic relaxation time or time constant τ is $\tau = RC$. In the frequency domain, the *RC* elements are separable due to the relation $\omega_{max}RC = 1$, which is in the impedance spectrum occurring at maximum loss frequency ω_{max}. From the impedance spectrum, it is possible to identify different *RC* elements, based on the capacitive values and assign them to appropriate regions of the test system. The values of the individual *R* and *C* components can be obtained.

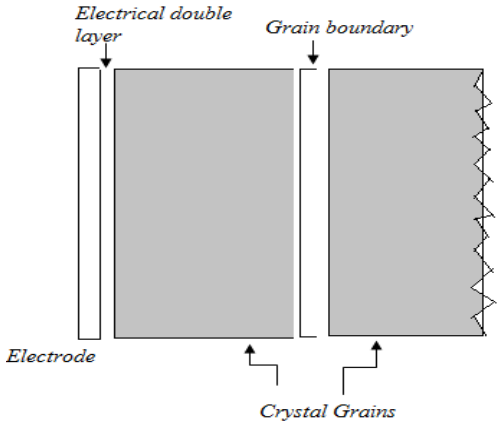

Figure (3.10): Maxwell's model of layered dielectric

Different physical features in the test system are represented by layers of varying thickness as in Maxwell's model of the layered dielectric as shown in figure (3.10). The model considers the permittivity of various regions, viz., surface layer near the electrode, grain boundary and grain. Various capacitance ranges are assigned for different regions, e.g., 10^{-12} F cm^{-1} for bulk, 10^{-11} F cm^{-1} to 10^{-8} F cm^{-1} for grain boundary and 10^{-7} F cm^{-1} to 10^{-5} F cm^{-1} for sample-electrode interface.

The ac response of the test system considers only the relationship between the applied voltage and the current through the test sample. The physical nature of the test sample, for example, single crystal, polycrystalline, blocking or non-blocking electrodes, etc. and its electrical properties, i.e., ionic, electronic or mixed conductor, ferroelectric, etc., are important for consideration. Plausible equivalent circuits, that is, some networking containing ideal resistive and reactive components may further be suggested which can represent these properties of the system and provide model for the collected data. The equivalent circuit shown in figure (3.11) is widely used to represent the bulk and grain boundary phenomenon in polycrystalline material.

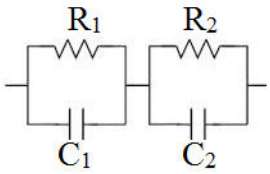

Figure (3.11): Equivalent circuit, subscripts 1 and 2 refer to bulk and grain boundary components

The present author has already discussed the impedance spectroscopy in detail in chapter-2, however, in this chapter the effect of bulk, grain and electrode, etc. is discussed, which will be used by the author for further discussion. In this regards the wonderful review by Sinclair [25] is worth noting.

Many workers have reported the impedance study on different materials, for example, potassium selective silicone rubber membranes [26], effect of Cr concentration on the electrical properties of SnO_2 based ceramics [27], CdS nanoparticles [28], lead free $(Na_{0.5}Bi_{0.5})TiO_3$ (NBT) ferroelectric ceramics [29], polycrystalline $CaBa_4SmTi_3Nb_7O_{30}$ [30], manganese mercury thiocyanate (MMTC) and cadmium mercury thiocyanate (CMTC) [31], polycrystalline $Pr_{0.8}Ca_{0.2}MnO_3$ [32] and polycrystalline $Pr_{0.4}Ca_{0.6}MnO_3$ [33]. Moreover, some other applications of impedance spectroscopy is reported. Younas et al [34] employed impedance

spectroscopy to investigate the dielectric and electric transport phenomenon in CuO nano-grains. They found John-Teller assisted polaronic hole hopping occurring in charge transport. Younas et al [35] identified secondary phases in Co-implanted ZnO single crystals by impedance spectroscopy.

In the present chapter, the impedance spectroscopy study is reported for the pure Pb and Pb-Fe mixed levo-tartrate crystals in the frequency range 100 Hz to 7 MHz.

Figure (3.12) shows the Nyquist diagram (Z'' vs. Z') at room temperature for pure Pb levo-tartrate crystals, while figure (3.13) shows the same diagrams for Pb-Fe mixed levo-tartrate crystals.

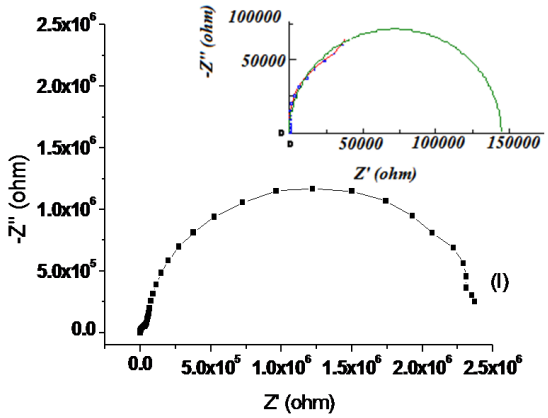

Figure (3.12): Nyquist plot for $PbC_4H_4O_6{\cdot}2.4H_2O$

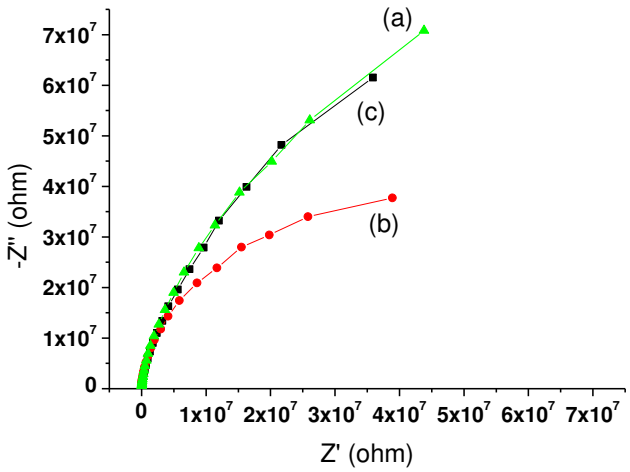

Figure (3.13): Nyquist plots for (a) Sample 3. $Pb_{0.989}Fe_{0.011}C_4H_4O_6{\cdot}1.9H_2O$
(b) Sample 4. $Pb_{0.993}Fe_{0.007}C_4H_4O_6{\cdot}0.5H_2O$ and
(c) Sample 5. $Pb_{0.994}Fe_{0.006}C_4H_4O_6{\cdot}0.17H_2O$

The best fit equivalent model circuit was obtained by the software Z-view. The value of grain resistance (R_g) and corresponding grain capacitance (C_g) as well as grain-boundary resistance (R_{gb}) and corresponding grain-boundary capacitance (C_{gb}) and relaxation frequency were also obtained by the software Z-view when data were simulated by the software Z-view to obtain the best fit equivalent circuit.

If these materials have two or more contributions with different relaxation times, then two or more circular arcs are observed in their complex plane impedance (*Z'' vs Z'*) plots [36-39]. A closer look of Nyquist plot of figure (3.12) near the origin clearly indicates the steep rising arc and a presence of a one more semi-circle near the origin, which can be viewed in detail manner by using the software Zview in the region near to the origin and shown in the inset of figure (3.12). The inset figure (3.12) indicates data point and curve by red color and the green line is fitting of the semicircle by the software. This small semicircle at high frequency indicates the effect of grain. The remaining large semicircle at low frequency indicates the grain boundary effect. The intercept of the semicircle on the real axis gives the resistance of grain (R_g) and grain boundary (R_{gb}) of the corresponding component contributing towards the impedance of the sample. This is represented in the form of two parallel *RC* elements in series as shown in figure (3.14). The two semi-circular arcs in the impedance plane plots show the presence of two relaxation process in the system with different relaxation frequencies. The low and high frequency arcs are attributed to the relaxation of the charge carriers at grain boundaries and grain interiors, respectively.

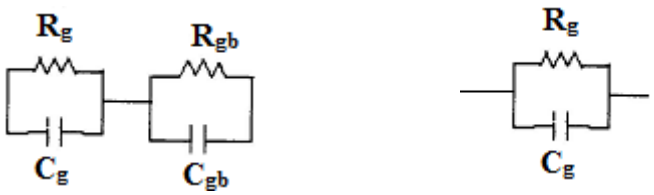

Figure (3.14): Equivalent circuit (a) for pure Pb levo-tartrate crystals (b) for mixed Pb-Fe levo-tartrate crystals

As the iron content is added into the pure Pb levo-tartrate sample, the high frequency semi-circular arc disappeared and only the initial part of the arc for all the three samples (II-IV) of Pb-Fe mixed levo-tartrate crystals exist, which is shown in the Nyquist plot of figure (3.13). Polycrystalline materials are heterogeneous in nature due to effects of grains and grain boundaries in the ac electrical properties [33]. Due to less thickness of grain boundaries compared to grain interiors, grain boundaries

offer high resistance. Therefore, larger is the product *RC* and lower would be the relaxation frequency. A parallel *RC* combination *(R_g, C_g)*, shown in Fig. 6(b), was found to have excellent fit with the experimental data, there by indicating the contribution from grains of the samples. The centers of all the three semicircles lie below the real axis having comparatively large radii. The radius of the semicircle indicates the resistivity of the material [40]. There was no systematic change observed in the radii with the composition of the samples, indicating no systematic variation in the resistivity of the samples observed with the composition of the samples. This may be due to very low percentage weight (1.1% and less) of iron in the samples.

The values of R_g, R_{gb}, C_g, C_{gb} and relaxation frequency for the pure Pb levo-tartrate crystals and the values of R_g, C_g and relaxation frequency for the mixed Pb-Fe levo-tartrate crystals at room temperature are obtained by using the software and listed in table 3.8.

Table (3.8): Grain and grain boundary resistances and capacitances

Sample Name	R_g (MΩ)	R_{gb}(MΩ)	C_g (pF)	C_{gb} (pF)	Relaxation frequency
$PbC_4H_4O_6$ $2.4H_2O$	0.145	2.38	103	66.5	f_g = 10.6 kHz f_{gb} = 1 kHz
$Pb_{0.989}Fe_{0.011}C_4H_4O_6$ $1.9H_2O$	169	--------	16	--------	f_g = 55 Hz
$Pb_{0.993}Fe_{0.007}C_4H_4O_6$ $0.5H_2O$	86.2	--------	7.99	--------	f_g = 229 Hz
$Pb_{0.994}Fe_{0.006}C_4H_4O_6$ $0.17H_2O$	210	--------	9.03	--------	f_g = 82 Hz

With comparison of pure lead tartrate crystals the values of grain resistances are high and indicate the clear effect of presence of additive. In the Nyquist curve of pure lead tartrate, the equivalent circuit shows the effect of both grain and grain boundaries, while in the mixed lead-iron levo tartrate the equivalent circuit shows the effect of increasing grain resistances and absence of grain boundary resistances. It is found that the majority amount of iron enters the crystalline lattice due to substitutional nature of iron and the grain resistance changes. There is a marked change in the electrical properties and equivalent circuits found with comparison to pure lead levo tartrate on addition of iron. It is observed from the table (3.8) that there is no systematic variation in the values of grain resistances for Pb-Fe mixed levo

tartrate, which may be due to the combine role of water of hydration/moisture and very low percentage weight of iron in the sample.

3.4.7 Dielectric studies

Dielectric study is important part of materials characterizations, because it does not only throw light on the materials behavior under the influence of applied electric field but also its applications. It becomes really interesting case when alternating fields are applied in place of static fields. In general, for any molecules, there will be two possibilities when influenced by an external field,

(i) Molecules may have permanent dipole moments which may be aligned in an external field.

(ii) The distances between ions or atoms may be influenced by external fields.

However, the polarization in atoms or molecules is induced by an external field by displacing electrons with respect to the corresponding nuclei. The electric properties of molecules are generally characterized by three quantities;

(i) The polarizability due to electronic displacement within composing atoms or ions.

(ii) The polarizability due to atomic or ionic displacement within the molecules (changes in bond angles and inter-atomic distances)

(iii) A permanent dipole moment.

Notwithstanding, the discussion becomes more interesting when solid material is considered for dielectric study for both static and alternating fields. This may lead to some interesting phenomena like piezoelectric effect, pyroelectric effect of ferroelectric effect in certain crystals. This has brought novel applications of various materials in science and technology.

A few authors reported the dielectric studies in the tartrate compounds. In 1990, Gon [41] has detected ferroelectric properties in calcium tartrate crystals. Lopez et al. [42] reported dielectric studies on gel grown zinc tartrate single crystals. Dabhi et al. [43] have reported dielectric study of gel grown zinc tartrate crystals. Later on, several other tartrate compounds have been investigated by dielectric study by applying an ac electric field, for instance, zinc tartrate [42,43], strontium tartrate [44], Mn^{+2} doped [45] and Cu^{+2} doped [46] calcium levo-tartrate, ytterbium tartrate trihydrate [23], ternary systems of Fe-Mn-Co levo-tartrate [3] and Fe-Mn-Ni levo-tartrate [4] and recently on Mn-Cu levo-tartrate [15]. In all these studies a smooth

decrease in the value of dielectric constant with increase in the frequency of applied field is observed.

In the present study, the dielectric constant of pure and mixed Pb-Fe levo-tartrate crystals was determined from the value of pellet dimensions and real and imaginary part of impedance. The following formulations have been used:

$$\varepsilon' = \frac{t}{\omega A \varepsilon_0} \frac{Z''}{Z'^2 + Z''^2} = \frac{t}{2\pi f A \varepsilon_0} \frac{Z''}{Z^2} \tag{3.2}$$

$$\varepsilon'' = \frac{t}{2\pi f A \varepsilon_0} \frac{Z'}{Z^2} \tag{3.3}$$

Where, A = Cross-section area of the pellet, t = Thickness of the pellet, ε_0 = Permittivity of free space = 8.854×10^{-12} F/m and $Z^2 = Z'^2 + Z''^2$.

The variation of dielectric constant and loss with frequency is shown in the figure (3.15) and (3.16) for pure Pb levo-tartrate crystals, respectively and figure (3.17) and (3.18) for mixed Pb-Fe levo-tartrate crystals, respectively.

It is seen that the values of both dielectric constant and dielectric loss decreases with increase in frequency, which is a common feature in many compounds such as iron-nickel-manganese ternary levo-tartrate crystals [4], zinc tartrate [43], 4-(2-hydroxyphenylamino)-pent-3en-2-one (HPAP) [47], and zinc doped nano-hydroxyapatite [48].

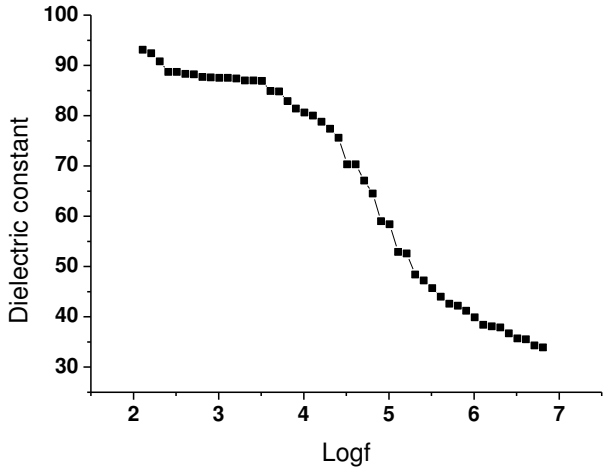

Figure (3.15): Plot of dielectric constant vs. log(f) for pure $PbC_4H_4O_6 \cdot 2.4H_2O$

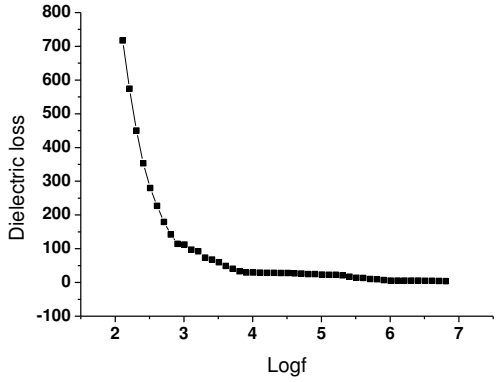

Figure (3.16): Plot of dielectric loss vs. log(f) for pure $PbC_4H_4O_6 \cdot 2.4H_2O$

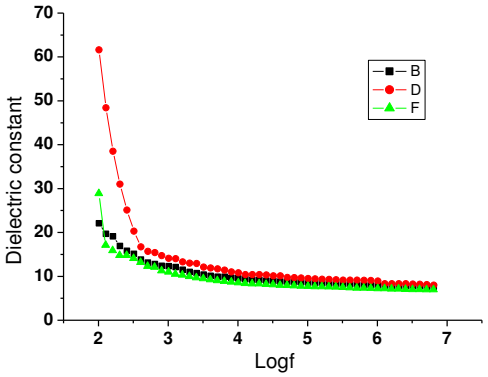

Figure (3.17): Plot of dielectric constant vs. log(f) for (B) Sample 3. $Pb_{0.989}Fe_{0.011}C_4H_4O_6 \cdot 1.9H_2O$ (D) sample 4. $Pb_{0.993}Fe_{0.007}C_4H_4O_6 \cdot 0.5H_2O$ and (F) sample 5. $Pb_{0.994}Fe_{0.006}C_4H_4O_6 \cdot 0.17H_2O$

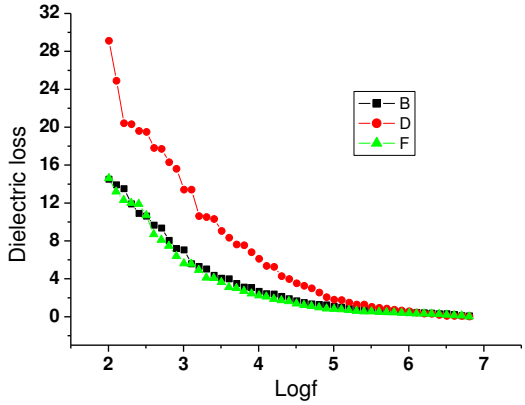

Figure (3.18): Plot of dielectric loss vs. log(f) for (B) Sample 3. $Pb_{0.989}Fe_{0.011}C_4H_4O_6 \cdot 1.9H_2O$ (D) sample 4. $Pb_{0.993}Fe_{0.007}C_4H_4O_6 \cdot 0.5H_2O$ and (F) sample 5. $Pb_{0.994}Fe_{0.006}C_4H_4O_6 \cdot 0.17H_2O$

The high value of dielectric constant at lower frequencies may be due to the presence of all the four types of polarizations, viz., electronic, ionic, orientation and space charge polarizations, but the low value of dielectric constant at higher frequencies is due to the loss of significance of some of these polarizations gradually. At low frequencies, the dipoles can easily switch their alignments with the changing field. As the frequency increases, both the dielectric constant and dielectric loss values are found to decrease exponentially and attain lower values which indicate that the dipoles do not comply with oscillating electric field and maintain their phase, thus they reduce their contribution to the polarization. The low power dissipation in the crystals is indicated by low dielectric loss values at higher frequencies. In the dielectric measurements as the capacitance is proportional to the dielectric constant, the addition of iron reduces the grain capacitance of Pb levo tartarte, which further results in the reduction of dielectric constant of the mixed Pb-Fe levo tartrate crystals. With comparison to pure lead levo tartrate crystals the dielectric loss is very low in lead- iron mixed levo tartrate crystals is due to the presence of iron at grain position reduces the grain capacitance and ultimately the dielectric loss. It is observed from the figure (3.17) that the dielectric constant changes in non-systematic manner with the different composition of the samples, which may be due to the combine role of water of hydration/moisture and composition of the sample. However, with comparison to pure lead tartrate the values of dielectric constants are low.

The value of ac conductivity σ_{ac} is calculated by using following formula [29].

$$\sigma(\omega) = \omega\varepsilon_o\varepsilon'' \quad (3.4)$$

Here, σ is the real part of the conductivity, ω is the angular frequency, ε_o is the Permittivity of free space = 8.854×10^{-12} F/m and ε'' is the imaginary part of the dielectric constant.

The ac resistivity ρ_{ac} is obtained from the expression $\rho_{ac} = 1/\sigma_{ac}$ (3.5)

Figure (3.19) shows the plots of ac conductivity versus log of frequency of applied field, which suggest that the values of the conductivities for the respective samples are constant for the lower values of applied frequency and high value of conductivity for the higher values of frequency. For pure Pb tartrate crystals, the value of conductivity is found high but as iron is doped, the value of conductivity is decreased. No major change is found in the value of conductivity with the change in

iron content in the samples, which may be due to the presence of over all very low percentage weight of iron in the mixed crystals of Pb-Fe levo-tartrate.

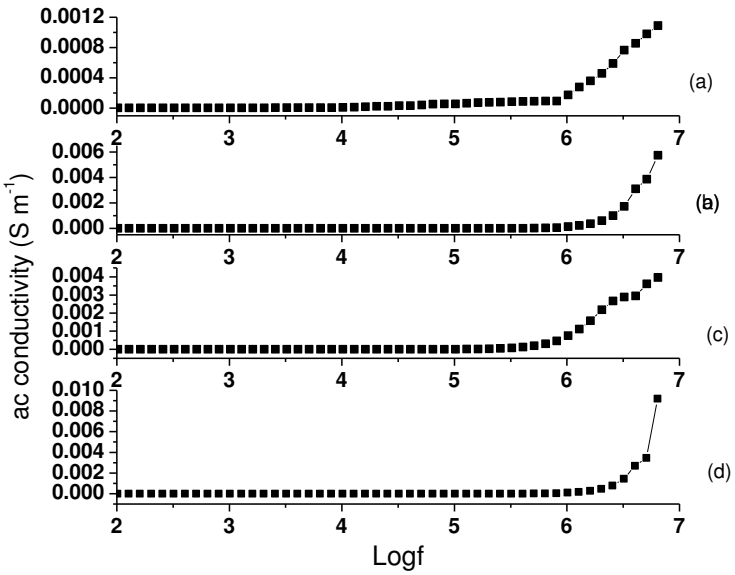

Figure (3.19): Plot of conductivity versus logf (a) $PbC_4H_4O_6$ $2.4H_2O$ sample-1 (b) $Pb_{0.989}Fe_{0.011}C_4H_4O_6 \cdot 1.9H_2O$ sample-3, (c) $Pb_{0.993}Fe_{0.007}C_4H_4O_6 \cdot 0.5H_2O$ sample-4 and (d) $Pb_{0.994}Fe_{0.006}C_4H_4O_6 \cdot 0.17H_2O$ sample-5

Want et al [49] suggested protonic conduction in gadolinium tartrate trihydrate from the data of variation of ac conductivity with temperature. On the other hand, Arora et al [50] suggested from the ac and dc conductivity data that strontium tartrate trihydrate possess conductivity between semiconductor and insulator and they suggested Efros-Shklovskii hopping occurring for conduction.

Figure (3.20) shows the plots of resistivity versus log of frequency of applied field. It can be noticed from the plots that the ac resistivity decreases with increase in the frequency for all the samples. No systematic variation in the order of the plots is observed for different sample compositions.

Electrical conductivity of solid electrolytes as a function of frequency can generally be described as frequency independent, dc conductivity σ_{dc} and a strongly frequency dependent ac conductivity σ_{ac} components. A typical frequency dependence of conductivity spectrum is shown in the figure (3.21), which exhibits three distinguished regions: (a) low frequency dispersion, (b) an intermediate frequency plateau and (c) an extended dispersion at high frequency [51-55]. The variation of

conductivity in the low frequency region is attributed to the polarization effects at the electrode and electrolyte interface.

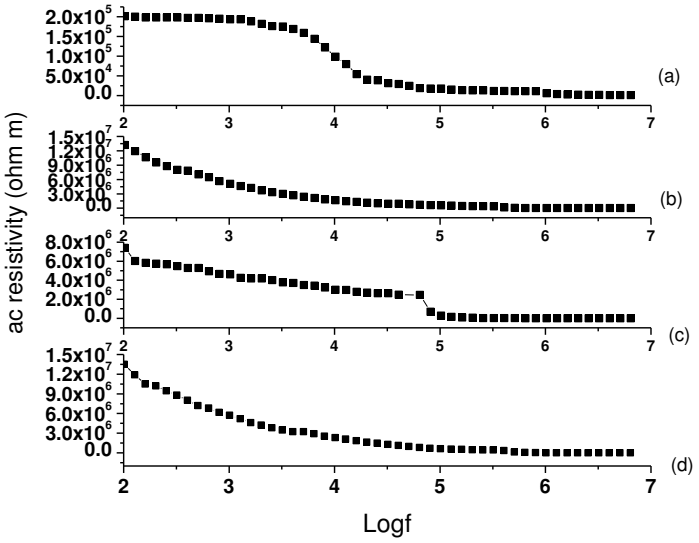

Figure (3.20): Plot of resistivity versus logf (a) $PbC_4H_4O_6$ 2.4H_2O sample-1 (b) $Pb_{0.989}Fe_{0.011}C_4H_4O_6$·1.9$H_2O$ sample-3, (c) $Pb_{0.993}Fe_{0.007}C_4H_4O_6$·0.5$H_2O$ sample-4 and (d) $Pb_{0.994}Fe_{0.006}C_4H_4O_6$·0.17$H_2O$ sample-5

In the low frequency region, more charge accumulation occurs at the electrode and electrolyte interface and hence, a drop in conductivity is observed. In the intermediate frequency plateau region, conductivity is almost found to be frequency independent and is equal to dc conductivity σ_{dc}. In the high frequency region, the conductivity increases with the frequency.

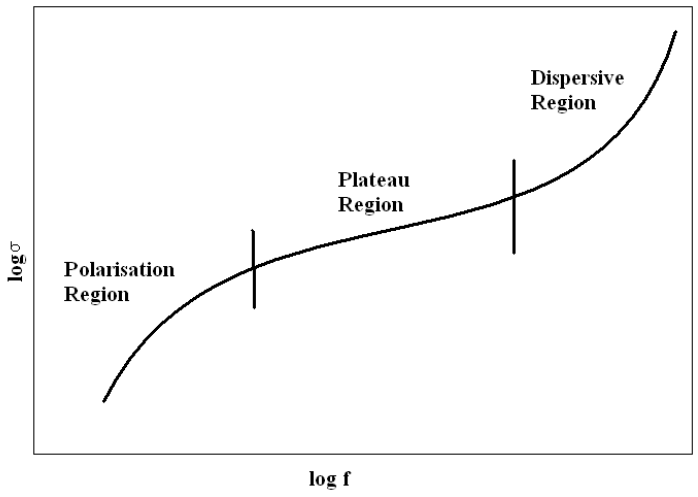

Figure (3.21): schematic representation of log conductivity versus frequency

The frequency dependence of conductivity or so – called universal dynamic response of ionic conductivity is related by a simple expression given by Jonscher's power law [53]

$$\sigma_{total}(\omega,T) = \sigma_{dc}(T) + \sigma_{ac}(\omega) = \sigma_{dc}(T) + A(T)\omega^{n} \quad (3.6)$$

where, σ_{dc} is the dc conductivity due to excitation of electron from a localized state to the conduction band, $A(T)\omega^{n}$ is the ac conductivity due to the dispersion phenomena occurring in the material, *A(T)* is a factor that depends on temperature but not on ω and *n* is the power law exponent, which generally varies between 0.6 and 1, depending on temperature [56]. The exponent *n* represents the degree of interaction between mobile ions with the lattice around them and *A* determines the strength of polarizability [57].

Figure (3.22) shows the Jonscher's plots for pure and mixed Pb-Fe levo-tartrate crystals.

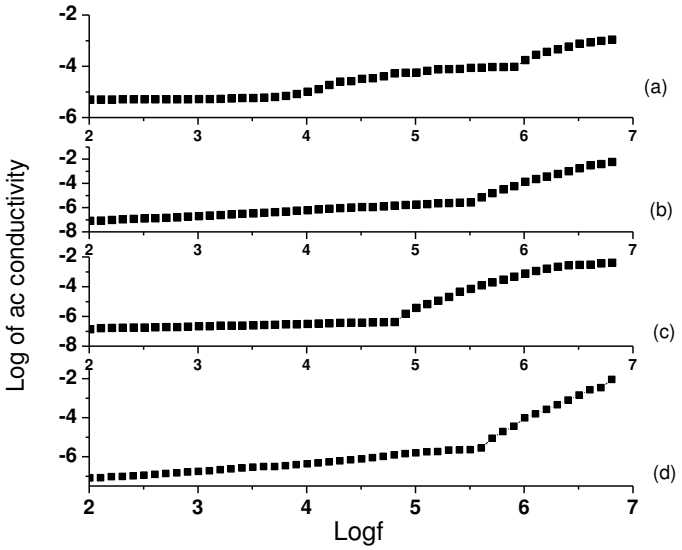

Figure (3.22): Jonscher's plot (a) $PbC_4H_4O_6$ $2.4H_2O$ sample-1 (b) $Pb_{0.989}Fe_{0.011}C_4H_4O_6 \cdot 1.9H_2O$ sample-3, (c) $Pb_{0.993}Fe_{0.007}C_4H_4O_6 \cdot 0.5H_2O$ sample-4 and (d) $Pb_{0.994}Fe_{0.006}C_4H_4O_6 \cdot 0.17H_2O$ sample-5

It is clear from the plot that the conductivity remains constant for the pure and mixed Pb-Fe levo-tartrate crystals in the low frequency region. Therefore, the relation $\sigma(\omega,T)\ \alpha\ \sigma_{dc}(T)$ holds well for all the samples in the low frequency region. Thereafter, as the frequency increases, indicating the relation $\sigma(\omega,T)\ \alpha\ \omega^{n}$ holds

well for all the samples. The values of exponent *n* and intercept *A* for all the samples are listed in table (3.9). A plot of ac conductivity versus angular frequency on log scale yields the value of exponent *n* and constant *A*.

The dc conductivity σ_{dc} for the pure Pb levo-tartrate crystals (sample-1) has been calculated using the relation $\sigma_{dc} = \frac{t}{R_b A}$ (3.7)

where, R_b is the grain (bulk) resistance, *t* and *A* are the thickness and surface area of the sample respectively [30]. It is found that the dc conductivity value calculated by using the above relation and the dc conductivity obtained from the Jonscher's plot are same and listed in the table (3.9) for the sample-1.

Table (3.9): The values of *n*, *A* and σ_{dc}

Sample	*n*	*A* (S m^{-1} rad^{-n})	σ_{dc} (S m^{-1}) (from formula)	σ_{dc} (S m^{-1}) (from plot)
$PbC_4H_4O_6$ $2.4H_2O$	0.62	4.38×10^{-8}	5.09×10^{-6}	5.04×10^{-6}
$Pb_{0.989}Fe_{0.011}C_4H_4O_6 \cdot 1.9H_2O$	0.90	2.78×10^{-10}	9.0×10^{-8}	8.53×10^{-8}
$Pb_{0.993}Fe_{0.007}C_4H_4O_6 \cdot 0.5H_2O$	0.95	2.13×10^{-10}	1.66×10^{-7}	1.02×10^{-7}
$Pb_{0.994}Fe_{0.006}C_4H_4O_6 \cdot 0.17H_2O$	0.88	2.72×10^{-10}	8.02×10^{-8}	8.59×10^{-8}

It can be observed form the values of *n* and A that the degree of interaction of mobile ions with the lattice as well as the strength of polarizability are almost the same for the mixed Pb-Fe levo-tartrate crystals, indicating effect of composition is not significant because the variation of Fe in the sample is from 1.1% to 0.6% and gives no major contribution. But in the pure lead levo tartrate sample the value of *n* is comparatively low and the value of A is comparatively high. The high value of A for pure lead tartrate crystals indicates high strength of polarizability; i.e., the dipoles per unit volume in pure Pb levo-tartrate crystals can align well in the direction of applied varying electric field is higher compared to the mixed Pb-Fe levo-tartrate crystals. As it has been already noted in section 3.4.1 of this chapter, the ionic radius of Pb is almost double the radius of Fe, the incorporation of Fe in Pb deforms the structure, alters the bonds and produces the strain; this is expected to reduce dielectric constant and on the other hand, increased the grain (bulk) resistance.

The polarizability of an atom or molecule depends on its dimension, as per the simple estimate for spherical atom or molecule the polarizability is proportional to the cube of its radius [58]. The higher value of ionic radius of Pb (1.19Å) compared to

Fe (0.55 Å) leads higher polarizability of lead than iron. As the polarizability is related to the dielectric constant by the following relation:

$$\alpha = \varepsilon_0(K - 1)/n \quad (3.8)$$

Where, α = Strength of Polarizability, K = Dielectric Constant, n = Number density

The above equation suggests that higher the value of dielectric constant, the higher is the polarizability. The higher value of polarizability of lead confirms the high value of dielectric constant of pure Pb levo tartrate crystals than mixed Pb-Fe levo tartrate crystals. As iron is added into the pure Pb levo tartrate crystals, the value of A in Jonscher's equation is reduced, indicating low polarizability and dielectric constant [59]. This is in correspondence to the impedance spectroscopy study results.

Funke [60] explained the physical significance of n in Jonscher's equation in two different regimes, i.e., $n \leq 1$ would indicate that the hopping motion involved is a translational motion with a sudden hopping and $n > 1$ would mean that the motion involved is a localized hopping of the species with a small hopping without leaving the neighborhoo [61]. Usually, in case of ionic conductors, the value of n can lie between 1 and 0.5 indicating the ideal long range pathways and diffusion limited hopping (tortuous pathways) [62]. Moreover, the Jump Relaxation Model (JRM) developed by Funke and Riess [63] attributes the dispersion in the conductivity to strong forward-backward jump correlations in the motion of ions. According to this model, after a hop of a central ion from initially relaxed local configurations, it is no longer in equilibrium with its surroundings. In order to stabilize the new position of the ion, the other ions and their environments have to move. On the other hand, the ion can also jump back in order to partially relax the configuration after the jump. The longer the ion stays in the new position after the jump, the lesser the preference to jump backward.

The variation of dielectric constant is within the values of 93 to 34 for sample (1), 22 to 7.7 for sample (3), 61 to 8 for sample (4) and 28 to 6.7 for sample (5). This variation is measured within the frequency range 100 Hz to 7 MHz. Singh and Ulrich [64] classified various dielectric materials according to the values of dielectric constant, that is, the high dielectric materials have $K > 7$ and the low dielectric materials having $3.9 > K$. Comparing the dielectric results with this classification, the present samples possess high values of dielectric constant and they may find the

application mainly in three areas such as memory cell dielectrics, gate dielectrics and passive components [64] after complete electrical and physical characterizations.

3.4.8 Vibrating Sample Magnetometer (VSM) study

According to modern theories the magnetism is inseparable from quantum mechanics. The magnetic moment of a free atom has three principal sources; the spin with which electrons are endowed; their orbital angular momentum about the nucleus; and the change in the orbital moment induced by an applied magnetic field. The first two effects give paramagnetic contributions to the magnetization, and the third gives a diamagnetic contribution [65]. Substances with a negative magnetic susceptibility are called diamagnetic; on the other hand, substances with positive magnetic susceptibility are called paramagnetic. Many standard books described various theories in details [66-69].

Magnetic properties of a variety of materials have been investigated. Raina [70] studied the magnetic properties of neodymium tartrate by using Gouy's method. The magnetic susceptibility of ferroelectric magnesium hydrogen phosphate crystals has been reported by Desai et al. [71]. Also, the magnetic behavior of vivianite ($Fe_3(PO_4)_2.8H_2O$) [72] and ludlomite ($Fe_3(PO_4)_2.4H_2O$) [73] have been investigated. Magnetic moment and susceptibility measurements have been investigated on mixed rare earth oxalate crystals [74]. Magnetic properties of copper chloride hydroxide hydrate $Cu_3Cl_4(OH)_2.2H_2O$ was investigation by Asaf et al. [75]. This has shown interesting behaviour, a weak ferromagnetic signal at T_N = 17.5 K has been observed in the *FC* branch of d.c. magnetic susceptibility. By using the VSM technique several workers in the present author's laboratory have reported magnetic susceptibility values of various tartrate compounds earlier, such as manganese tartrate [76], Iron (II) tartrate [7], mixed iron-cobalt tartrate and mixed iron-nickel tartrate [7], copper tartrate, zinc tartrate and cadmium tartrate [77], iron-mangenese-cobalt ternary tartrate [3] and iron-mangenese-nickel ternary tartrate [78]. Mathivanan and Haris [79] reported magnetic susceptibility of copper doped iron tartrate crystals by Guoy balance. Very recently, the magnetic susceptibility of gel grown cobalt tartrate is reported by the Gouy balance [80].

In the present investigation, the magnetic moments of Pb-Fe mixed levo-tartrate crystals have been measured by using the Vibrating Sample Magnetometer (VSM) at room temperature at different applied magnetic field from 0.05 Tesla to 1.5

Tesla. The powdered samples were used. The bulk magnetic susceptibility was calculated from magnetic moment.

Table (3.10), (3.11) and (3.12) indicate the variation in magnetic moment and bulk susceptibility with different applied magnetic fields for the samples $Pb_{0.989}Fe_{0.011}C_4H_4O_6 \cdot 1.9H_2O$, $Pb_{0.993}Fe_{0.007}C_4H_4O_6 \cdot 0.5H_2O$ and $Pb_{0.994}Fe_{0.006}C_4H_4O_6 \cdot 0.17H_2O$, respectively, at room temperature. It can be seen that all the samples are paramagnetic in nature.

The electronic configuration of Pb (II) cation is $[Xe]6S^2 4f^{14} 5d^{10}$. Iron belongs to transition metals, the electron configuration of Fe (II) and Fe (III) cations are $[Ar]3d^6$ and $[Ar]3d^5$, respectively. There are no unpaired *(n-1)d* electrons in Pb (II) cations, therefore, it is diamagnetic in nature. While, in the ionization of transition metals the *ns* electrons are lost before *(n-1)d* electrons. All the common transition metals lose their *ns* electrons first and the cations formed have the electronic configurations of the general type (noble gas core) $(n-1)d^x$. This point is important because the magnetic properties of transition metal cations are determined by the number of unpaired five electrons. Fe^{+3} is paramagnetic to the extent of five unpaired electrons. Therefore, the doping of Fe into Pb levo-tartrate results into the paramagnetic behavior of mixed Pb-Fe levo-tartrate crystals.

Table (3.10): Magnetic moment data for $Pb_{0.989}Fe_{0.011}C_4H_4O_6 \cdot 1.9H_2O$

Applied Magnetic Field (Tesla)	Magnetic moment (emu) × 10^{-4}	Bulk Susceptibility (Am^2/ kg. T) × 10^{-2}
0.05	1.13	4.25
0.1	2.67	5.04
0.2	5.69	5.37
0.3	8.78	5.52
0.4	11.7	5.52
0.5	14.8	5.58
0.6	17.9	5.62
0.7	20.5	5.54
0.8	23.3	5.50
0.9	26.1	5.48
1.0	29.3	5.53
1.1	32.5	5.58
1.2	35.2	5.53
1.3	38.4	5.58
1.4	41.7	5.63
1.5	45.1	5.67

Table (3.11): Magnetic moment data for $Pb_{0.993}Fe_{0.007}C_4H_4O_6 \cdot 0.5H_2O$

Applied Magnetic Field (Tesla)	Magnetic moment (emu) × 10^{-4}	Bulk Susceptibility (Am^2/ kg. T) × 10^{-2}
0.05	0.833	3.79
0.1	2.04	4.64
0.2	4.80	5.46
0.3	7.01	5.31
0.4	9.22	5.24
0.5	11.3	5.14
0.6	13.9	5.28
0.7	18.3	5.95
0.8	22.9	6.51
0.9	25.8	6.53
1.0	28.9	6.56
1.1	32.8	6.77
1.2	35.4	6.71
1.3	38.5	6.73
1.4	42.1	6.83
1.5	45.3	6.86

Table (3.12): Magnetic moment data for $Pb_{0.994}Fe_{0.006}C_4H_4O_6 \cdot 0.17H_2O$

Applied Magnetic Field (Tesla)	Magnetic moment (emu) × 10^{-4}	Bulk Susceptibility (Am^2/ kg. T) × 10^{-2}
0.05	1.36	4.30
0.1	3.01	4.78
0.2	5.87	4.66
0.3	8.67	4.59
0.4	11.6	4.62
0.5	14.4	4.56
0.6	17.6	4.65
0.7	20.2	4.58
0.8	22.3	4.43
0.9	26.5	4.67
1.0	27.9	4.43
1.1	30.8	4.45
1.2	34.1	4.51
1.3	38.4	4.69
1.4	40.2	4.56
1.5	42.9	4.54

It is observed that the different proportion of Fe has no effect on the value of magnetic moment and bulk susceptibility. This may be due to very less percentage weight of Fe in the mixed crystals of Pb and Fe. Different amount of water is associated with Pb-Fe levo-tartrate crystals and water being diamagnetic in nature affects the net bulk magnetic property.

3.5 Conclusions

(1) Pure and mixed lead–iron levo-tartrate crystals have been grown by single diffusion gel growth technique.

(2) A thick band of white, dendrite type, long crystals of pure lead tartrate was observed at the gel-liquid interface due to the high concentration of reactant used.

(3) Dendrite crystals of varying number density and coloration were obtained for mixed Pb-Fe levo-tartrate crystals which depended on the composition and the content of Pb and Fe.

(4) Powder XRD study suggested that pure Pb levo-tartrate and mixed Pb-Fe levo-tartrate crystals possessed orthorhombic crystal structure. As the iron content was within 1.07%, the unit cell parameter values of mixed Pb-Fe levo-tartrate crystals were closer to the unit cell parameter values of pure lead levo-tartrate.

(5) From FTIR spectra of pure and mixed Pb-Fe levo-tartrate crystals, the presence of water of hydration, C=O, C-H, C-O, C-C functional groups and metal-oxygen group were confirmed. It was observed that there was no significant effect of iron on the different absorptions except the minor shifting is observed towards lower frequency in O-H and Metal-Oxygen vibrations. This may be due to very less mount of iron in the mixed Pb-Fe levo-tartrate crystals.

(6) From EDAX and TGA analysis the exact formulae of pure and mixed Pb-Fe levo-tartrate crystal were determined with estimation of lead and iron content and water of hydration as well. The hydrated radii of Pb and Fe are important to determine the amount of Pb and Fe in the mixed crystals.

(7) Pure and mixed Pb-Fe levo-tartrate crystals were thermally unstable and on heating they became anhydrous and finally decomposed into oxides

through the carbonate stage. The amount of water of hydration was determined.

(8) The thermodynamic parameters for different exothermic processes of Pb levo-tartrate and mixed Pb-Fe levo-tartrate crystals were obtained from the software available with the thermal analyzer.

(9) The impedance study of pure and mixed Pb-Fe levo-tartrate crystals showed that the pure Pb levo-tartrate crystals exhibited two semicircles, indicating the presence of gain and grain boundary effects, which is represented in the form of two parallel RC elements in series. While the mixed Pb-Fe levo-tartrate crystals exhibited single semicircles, indicating the presence of grain effects only, this is represented in the form of single RC element.

(10) The dielectric constant and loss both decreased with increasing frequency. The dielectric constant changed in non-systematic manner with the different composition of the samples, which may be due to the combine role of water of hydration/moisture and composition of the samples.

(11) The values of ac conductivity and ac resistivity were calculated. The plots of ac conductivity versus frequency of applied field suggested that as the frequency increased, the conductivity increased. The ac conductivity was due to the hopping motion with the ideal long range and diffusion limited pathways of charge carriers. However, the opposite nature was obtained for ac resistivity.

(12) It was also observed that the Jonscher's law obeyed by all the samples. As the ionic radius of Fe is quite smaller than Pb, the doping of Fe is affecting the bond length and deforms the structure resulting into the local strain. This reduced the dielectric constant; while increased the grain (bulk) resistance.

(13) The values of the bulk magnetic susceptibility were determined by VSM for mixed Pb-Fe levo-tartrate crystals. The crystals exhibited paramagnetic nature, which might be due to presence of iron ligand. The different proportion of iron had no significant effect on the values of susceptibility. The different amount of water associated with crystals might influence the bulk magnetic susceptibility due to its diamagnetic nature.

References

[1] S. J. Joshi, B. B. Parekh, K. D. Vora and M. J. Joshi; *Bull. Mater. Sci.,* **29(3)** (2006) 307-312.

[2] K. D. Parikh, B. B. Parekh, D. J. Dave and M. J. Joshi; *Indian J. Phys.,* **80(7)** (2006) 719-726.

[3] S. J. Joshi, K. P. Tank, B. B. Parekh and M. J. Joshi; *Cryst. Res. Technol.,* **45** (2010) 303-310.

[4] S. J. Joshi, K. P. Tank, B. B. Parekh and M. J. Joshi; *J. Therm. Anal. Calorim.,* **112** (2013) 761-766..

[5] D. K. Sawant, H. M. Patil, D. S. Bhavsar, J. H. Patil and K. D. Girase; *J. Therm. Anal. Calorim.,* 10.1007/s10973-011-1600-z (2011).

[6] S. Joseph; *Ph.D. Thesis*, Saurashtra University, Rajkot (1997).

[7] S. B. Kansara, *M.Phil. Dissertation*, Saurashtra University, Rajkot (2003).

[8] S. Joseph and M. J. Joshi; *Indian J. Phys.*, **71A** (1997) 183.

[9] S. Joseph, H. S. Joshi and M. J. Joshi; *Cryst. Res. Technol*., **32** (1997) 339.

[10] M. Abdulkadhar and M. A. Ittyachen; *J. Cryst. Growth,* **39** (1977) 365.

[11] H. O. Jethva and M. V. Parsania; *Asian J. Chem.,* **22(8)** (2010) 6317-6320.

[12] G. Lillybai and M. H. Rahimkutty; *J. of Atomic, Mol. & Opt. Phy.,* DOI: 10.1155/2010/265403 (2010).

[13] Dove and Nix; *Geochimica et Cosmochimica Acta.,* **61** (1997) 3331.

[14] C. F. Albert, G. Wilkinson and P. L. Gaus; *"Basic Inorganic Chemistry",* 3rd ed., John Wiley and Sons, p. no. 292 (1995).

[15] S. J. Joshi, K. P. Tank, P. M. Vyas and M. J. Joshi; *J. Cryst. Growth.,* **401** (2014) 201-214.

[16] D. J. A. De Ridder, K. Goubitz, E. J. Sonneveld, W. Molleman and H. Schenk; *Cryst. Struct. Commun.*, **C58** (2002) 596-598.

[17] B. D. Cullity; *"Elements of x-ray diffraction",* Addison-Wesley Publishing Co., p. no. 447 (1978).

[18] J. Bolard; *J. Chim. Phys.,* **62** (1965) 894.

[19] L. L. Sheveheko; *Zh. Neorg. Khim.,* **13** (1968) 143.

[20] M. C. Patel, A. Ray and A. Venkatraman; *J. Phys. Chem. Solids,* **58** (1997) 749.

[21] F. E. Mabbe and D. J. Machin; "*Magnetism and transition metal complexes*", Chapman and Hall, London (1973) 159.

[22] K. D. Vohra; M. Phil. Dissertation, Saurashtra University, Rajkot (2000).

[23] B. Want. F. Ahmed and P. N. Kotru; *J. Mater. Sci*. **42** (2007) 9324.

[24] E. M. Rodrigues, C. T. Carvalho, A. B. deSiqueira, G. Bannach, M. Ionqshiro; *Thermochimica Acta*, **496** (2009) 156.

[25] D. C. Sinclair; *Bol. Soc. Esp. Ceram. Vidrio.,* **34** (1995) 55.

[26] P. D. Van der Wal, E. J. R. Sudholter, B. A. Boukamp, H. J. M. Bouwmeester and D. N. Reinhoudt; *J. Electroanal. Chem.,* **317** (1991) 153.

[27] D. R. Leite, W. C. Las, G. Brankovic, M. A. Zaghete, M. Cilense and J. A. Varela; *Materials Science Forum,* **498-499** (2005) 337.

[28] J. S. Kim, B. C. Choi and J. H. Jeong; *J. of Korean Phys. Soc.,* **55(2)** (2009) 879.

[29] R. Tripathi, A. Kumar and T. P. Sinha; *Pramana J. Phys.,* **72(6)** (2009) 969.

[30] P. Ganguly and A. K. Jha; *Bull. Mater. Sci.,* **34(4)** (2011) 907.

[31] R. Josephine Usha, J. Arul Martin and V. Joseph; *Arch. Appl. Sci. Res.,* **4(1)** (2012) 638.

[32] M. Shah, M. Nadeem and M. Atif; *J. Appl. Phys.,* **112** (2012) 103718 1-8.

[33] M. Shah, M. Nadeem, M. Idress, M. Atif and M. J. Akhtar; *J. Magnetism & Magnetic Mater.,* **332** (2013) 61.

[34] M. Younas, M. Nadeem, M. Idress, M. J. Akhtar; *Appl. Phys. Lett.,* **100** (2012) 152103.

[35] M. Younas, L. L. Zou, M. Nadeem, Naeem-ur-Rehman, S. C. Su, Z. L. Wang, W. Anwand, A. Wagner, J. H. Hao, C. W. Leung, R. Lortz and F. C. C. Ling; *Phys. Chem. Chem. Phys.,* **16** (2014) 16030.

[36] D. C. Sinclair and A. R. West, *J. Appl. Phys.* **66(8)** (1989) 3850.

[37] J. R. MacDonald, *Impedance Spectroscopy*, Wiley, New York, 1987.

[38] D. C. Sinclair and A. R. West, *J. Mat. Sci. Lett.* **7** (1988) 823.

[39] F. D. Morrison and D. C. Sincalir, A. R. West, *J. Appl. Phys.* **86** (1999) 6355.

[40] A. K. Roy, K. Prasad and A. Prasad, *Process. & Appl. of Ceramics*, **7(2)** (2013) 81-91.

[41] H. B. Gon; *J. Cryst. Growth*, **102** (1990) 50.

[42] T. Lopez, J. Stockel, J. Peraza, M. E.Torres and A.C. Yanes; *Cryst. Res. Technol*., **30** (1995) 677.

[43] R. M. Dabhi, B. B. Parekh and M. J. Joshi; *Indian J. Phys*., **79(5)** (2005) 503.

[44] S. K. Arora, V. Patel, B. Amin and A. Kotharin; *Bull. Mater. Sci*., **27** (2004) 141 503.

[45] S. R. Suthar and M. J. Joshi; *Cryst. Res. &Tech.,***41** (2006) 664

[46] S.R. Suthar, S. J. Joshi, B. B. Parekh and M. J. Joshi; *Indian J.l of Pure & Appl. Phys.*, **45** (2007) 48.

[47] B. B. Parekh, D. H. Purohit, P. Sagayaraj, H. S. Joshi and M. J. Joshi, *Cryst. Res. & Technol*., **42** (2007) 407.

[48] K. P. Tank, P. Sharma, D. K. Kanchan and M. J. Joshi, *Cryst. Res. & Technol*., **46** (2011) 1309.

[49] B. Want, A. Farooq and P. N. Kotru; *Mater. Sci. & Engineering,* **38** (2007) 270.

[50] S. K. Arora, V. Patel, R. G. Patel, B. Amin and A. Kothari; *J. Phys. Chem. and Chem. Solids*, **65** (2004) 465.

[51] L. L. Hensch and J. K. West; *Principles of Electronic Ceramics,* John Wiley & Sons, Singapore (1990).

[52] A. K. Jonscher; *Phys. Thin Films,* **11** (1980) 23.

[53] A. K. Jonscher; *Nature,* **256** (1977) 673.

[54] A. K. Jonscher; *J. Mater. Sci.,* **16** (1981) 2037.

[55] M. D. Ingram; *Phys. Chem. Glasses,* **28** (1987) 215.

[56] J. O. López and R. G. Aguilar; *Rev. Mex. Fis.,* **49** (2003) 529.

[57] C. Karthik and K. B. R. Varma; *J. Phys. Chem. Solids,* **67 (2006)** 2437.

[58] R. Murugeshan, Electricity and magnetism, 7th ed., S. Chand, New Delhi (2008) p. 300.

[59] D. Shamiryan, T. Abell, F. Iacopi and K. Maex, *Materials today*, **7(1)** (2004) 34.

[60] K. Funke, *Prog. Solid State Chem.*, **22** (1993) 111.

[61] S. Sen and R.N.P. Choudhary, *Mater. Chem. Phys.*, **87** (2004) 256.

[62] K.A. Mauritz, *Macromolecules*. **22** (1989) 4483.

[63] K. Funke and I. Riess, *Z. Phys. Chem. Neue Folge*. **140** (1984) 217.

[64] R. Singh and R. K. Ulrich, High and low dielectric constant materials, 4th Symposium, The Electrochemical Society Interface, Summer (1999) 26.

[65] C. Kittel; *Introduction to Solid State Physics*, 5th Ed., Wiley Eastern, New Delhi (1989).

[66] R. M. White; *Quantum Theory on Magnetism*, Mc- Graw Hill (1970).

[67] L. F. Bates; *Modern Magnetism*, 4th Ed., Cambridge (1961).

[68] J. H. Van Vleck; *The Theory of Electric and Magnetic Susceptibilities*, Oxford (1932).

[69] B. D. Cullity; *Introduction to Magnetic Materials,* Addison-Wesley, Readings, Massachussetts (1972).

[70] K. K. Raina; *Ph. D. Thesis*, University of Jammu, Jammu (1985).

[71] C. C. Desai, K. N. Patel and M. J. Shukla; J. *Mater. Sci. Lett*., **8** (1989) 1391.

[72] H. C. Meijer, J. Van Den Handel and F. Frikkee; *Physica*, **34** (1967) 475.

[73] S. Paster, C. Wilkinson, J. B. Forsyth, C. E. Johnson, Q. A. Pankhurst and M. F. Thomas; *Hypperfine Interct*., **54** (1990) 651.

[74] C. Joseph, G. Varghese and M. A. Ittayachen; *Cryst. Res. and Technol*., **31** (196) 127.

[75] U. Asaf, D. Hechel and I. Felner; *Solid State Commun*., **98** (1996) 571.

[76] S. N. Bhatt*; M. Phil., Dissertation*, Saurashtra University, Rajkot (1997).

[77] R. M. Dabhi; *Ph. D. Thesis,* Saurashtra University, Rajkot (2003).

[78] S. J. Joshi; *Ph. D. Thesis,* Saurashtra University, Rajkot (2009).

[79] V. Mathivanan and M. Haris; *Pramana-J. of Phys.,* **81** (2013) 177.

[80] V. Mathivanan, M. Haris, T. Prasanyaa and M. Amgalan; *Pramana-J. of Phys.,* **82** (2014) 537.